Title

Distinct Spatiotemporally Dynamic Wnt-Secreting Niches Regulate Proximal Airway Regeneration and Aging

Journal

Cell Stem Cell, 27(3)

ISSN

1934-5909

Authors

Aros, Cody J
Vijayaraj, Preethi
Pantoja, Carla J
et al.

Publication Date

2020-09-01

DOI

10.1016/j.stem.2020.06.019

Peer reviewed

HHS Public Access

Author manuscript

Cell Stem Cell. Author manuscript; available in PMC 2021 September 03.

Published in final edited form as:

Cell Stem Cell. 2020 September 03; 27(3): 413–429.e4. doi:10.1016/j.stem.2020.06.019.

Distinct spatiotemporally dynamic Wnt-secreting niches regulate proximal airway regeneration and aging

Cody J. Aros[1,2,3], **Preethi Vijayaraj**[1,4], **Carla J. Pantoja**[1], **Bharti Bisht**[1,5], **Luisa K. Meneses**[1], **Jenna M. Sandlin**[1], **Jonathan A. Tse**[1], **Michelle W. Chen**[1], **Arunima Purkayastha**[1], **David W. Shia**[1,2,3], **Jennifer M.S. Sucre**[6], **Tammy M. Rickabaugh**[1], **Eszter K. Vladar**[7], **Manash K. Paul**[1,5], **Brigitte N. Gomperts**[1,2,4,5,8,9]

[1]UCLA Children's Discovery and Innovation Institute, Mattel Children's Hospital UCLA, Department of Pediatrics, David Geffen School of Medicine, UCLA, Los Angeles, CA, 90095, USA

[2]UCLA Department of Molecular Biology Interdepartmental Program, UCLA, Los Angeles, CA, 90095, USAs

[3]UCLA Medical Scientist Training Program, David Geffen School of Medicine, UCLA, Los Angeles, CA, 90095, USA

[4]Jonsson Comprehensive Cancer Center, UCLA, Los Angeles, CA, 90095, USA

[5]Division of Pulmonary and Critical Care Medicine, Department of Medicine, David Geffen School of Medicine, UCLA, Los Angeles, CA, 90095, USA

[6]Mildred Stahlman Division of Neonatology, Department of Pediatrics, Vanderbilt University, Nashville, TN, 37232, USA

[7]Division of Pulmonary Sciences and Critical Care Medicine, Department of Medicine and Department of Cell and Developmental Biology, University of Colorado Denver School of Medicine, Aurora, CO, 80045, USA

[8]Eli and Edythe Broad Stem Cell Research Center, UCLA, Los Angeles, CA, 90095, USA

[9]Lead Contact

Co-corresponding authors: Brigitte N. Gomperts (bgomperts@mednet.ucla.edu), Manash K. Paul (paul_cancerbiotech@yahoo.co.in), Phone number: (310) 206-0772.

AUTHOR CONTRIBUTIONS

C.J.A.: conception and design, collection and assembly of data, data analysis and interpretation, manuscript writing.
M.K.P.: conception and design, collection and assembly of data, data analysis and interpretation.
B.B.: collection and assembly of data, data analysis and interpretation.
P.V., L.K.M., C.J.P., A.P., D.W.S., T.M.R.: data analysis and interpretation and technical support.
J.M.S., J.A.T.: technical support.
J.M.S.S., E.K.V.: collection and assembly of data, data analysis and interpretation and technical support.
B.N.G.: conception and design, data analysis and interpretation, manuscript writing, final approval of the manuscript and financial support.

DECLARATION OF INTERESTS

The authors declare no competing interests.

SUMMARY

Our understanding of dynamic interactions between airway basal stem cells (ABSCs) and their signaling niches in homeostasis, injury, and aging remains elusive. Using transgenic mice and pharmacologic studies, we found Wnt/β-catenin within ABSCs was essential for proliferation post-injury *in vivo.* ABSC-derived Wnt ligand production was dispensable for epithelial proliferation. Instead, the PDGFRα+ lineage in the intercartilaginous zone (ICZ) niche transiently secreted Wnt ligand necessary for ABSC proliferation. Strikingly, ABSC-derived Wnt ligand later drove early progenitor differentiation to ciliated cells. We discovered additional changes in aging, as glandular-like epithelial invaginations (GLEIs) derived from ABSCs emerged exclusively in the ICZ of aged mice and contributed to airway homeostasis and repair. Further, ABSC Wnt ligand secretion was necessary for GLEI formation and constitutive activation of β-catenin in young mice induced their formation *in vivo.* Collectively, these data underscore multiple, spatiotemporally dynamic Wnt-secreting niches that regulate functionally distinct phases of airway regeneration and aging.

eTOC Blurb

Aros et al. unveil multiple dynamic Wnt/β-catenin signaling niches that govern murine airway proliferation and differentiation. They further extend these findings in the setting of aging to elucidate how Wnt/β-catenin niche activity regulates profound structural changes in the proximal airway.

Graphical Abstract

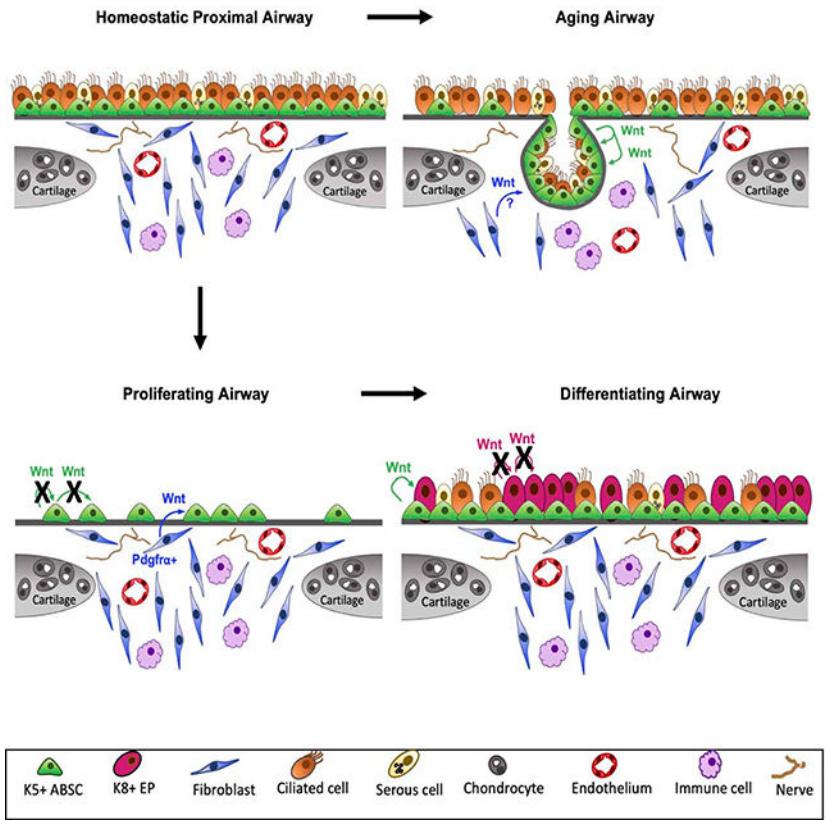

INTRODUCTION

The lung is a structurally and functionally intricate organ with several diverse cell types. Appreciable changes in the composition of the epithelial stem cell and mesenchymal cell compartments along the proximo-distal axis of the airway contribute to its striking complexity. At its most proximal portion, the cartilaginous conducting airways play a vital role in host defense that protects mammals from airborne pathogens. This is accomplished by a highly specialized simple pseudostratified mucociliary epithelium that arises from anatomically-defined, resident adult airway basal stem cells (ABSCs) marked by Keratin 5 (K5) expression (Cole et al., 2010; Hong et al., 2004; Montoro et al., 2018; Plasschaert et al., 2018; Rock et al., 2009; Schoch et al., 2004). In contrast, the non-cartilaginous bronchiolar, alveolar, and bronchioalveolar tissues of the airway have region-specific adult stem cell populations (Barkauskas et al., 2013; Desai et al., 2014; Kim et al., 2005; Rawlins et al., 2009) capable of self-renewal and differentiation.

Following injury, the tracheal repair response occurs in two distinct phases. Denuding of the epithelium triggers an initial proliferative expansion phase in which ABSCs undergo symmetric followed by asymmetric division that gives rise to K8+ early progenitors (Paul et al., 2014; Rock et al., 2011; Rock et al., 2009; Tata et al., 2013). A phase of differentiation then proceeds, ultimately leading to repair of the pseudostratified epithelium with the optimal proportion of ABSCs and mucociliary cells. Dysregulated repair can lead to a multitude of pathologies, including mucus metaplasia, ABSC hyperplasia, and stepwise

progression to squamous lung cancer (SqLC) (Hogan et al., 2014; Ooi et al., 2010). As such, developing a nuanced understanding of tracheal homeostatic mechanisms is of paramount importance.

Conducting airways of the trachea are lined with C-shaped cartilage rings that serve as a structural scaffold, equipping it with a rigidity that prevents its collapse. The subepithelial intercartilaginous zone (ICZ) of the airway harbors diverse cell types including but not limited to fibroblasts, endothelial cells, immune cells, and nerves that together have been speculated to comprise an intricate ABSC niche (Borthwick et al., 2001; Donne et al., 2015). Previous work observed that the epithelial surface above the ICZ contains a greater density of ciliated cells in comparison to regions above cartilage in the adult rodent trachea (Oliveira et al., 2003; Toskala et al., 2005). Efforts have also identified that the IL-6 from ICZ cells signals onto ABSCs to promote STAT3 activity and subsequently regulate ciliated cell formation from basal cells (Tadokoro et al., 2014). These findings implicate cell-cell communication between the ICZ and surface airway epithelium (SAE), however, the dynamics of this ICZ niche during injury repair and aging remain unexplored.

Recent studies have characterized the active epithelial-mesenchymal crosstalk in murine bronchiolar and alveolar homeostasis, of which Wnt signaling plays an increasingly defined role (Lee et al., 2017; Nabhan et al., 2018; Volckaert et al., 2011; Zepp et al., 2017). In the trachea, however, the effects of Wnt signaling on proliferation, differentiation, and injury repair are poorly understood. Prior work from others has suggested an importance for β-catenin in basal cell fate decisions (Giangreco et al., 2012; Malleske et al., 2018; Reynolds et al., 2008). However, current limitations in our understanding stem from a dearth of studies that dissect the spatiotemporally dynamic role of Wnt/β-catenin signaling during distinct phases of repair as well as aging and how this is contextualized within signaling niches *in vivo.*

Here, we employ several transgenic mouse models to dissect the dynamic mechanisms by which Wnt signaling modulates proximal ABSC homeostasis, injury repair, and aging *in vivo.* We show that canonical Wnt/β-catenin signaling is responsible for the proliferative phase of tracheal repair following injury *in vivo* and is mediated by phosphorylation of β-catenin protein at tyrosine 489. We reveal that a transiently activated Pdgfrα+ lineage in the ICZ marks a Wnt-producing niche necessary for driving proximal airway epithelial proliferation *in vivo.* The proximal airway then undergoes a dynamic cellular switch to form an intra-epithelial niche that directs differentiation to ciliated cells *in vivo,* as K5+ ABSCs secrete Wnt ligand to facilitate their formation. Importantly, the aging proximal airway ICZ niche is marked by the emergence of K5+ ABSC-derived glandular-like epithelial invaginations (GLEIs) that contribute to repair after injury and can be formed by constitutively activating Wnt/β-catenin signaling in the ABSCs of young mice. Our efforts thus demonstrate the spatiotemporal dynamism of Wnt signaling across multiple proximal airway niches that together act as critical regulators of distinct phases of regeneration as well as aging.

RESULTS

Canonical Wnt/β-catenin signaling is essential for proximal ABSC proliferation after injury *in vivo.*

At steady state, the mouse proximal airway epithelium has a slow turnover of approximately one ABSC every 7–10 days (Rock et al., 2010). As such, to study mechanisms of ABSC self-renewal, we employ an injury model whereby we administer intratracheal (i.t.) polidocanol to slough the proximal airway epithelium, as previously described (Borthwick et al., 2001; Paul et al., 2014). The few remaining ABSCs subsequently undergo an initial phase of symmetric division to repopulate the ABSCs. This is followed by a period of asymmetric division, during which ABSCs give rise to the optimal proportion of differentiated mucociliary cells. Previous work has shown that 48 hours post-injury (hpi) is the point of maximal proliferation following injury, with a notable decrease by 72hpi as differentiation commences (Paul et al., 2014).

As the role of Wnt signaling remains poorly understood in proximal ABSC homeostasis and injury repair *in vivo,* we sought to analyze its activity *in vivo.* Mice were administered i.t. polidocanol and sacrificed at 12, 24, 48, 72, and 96hpi (Figure 1A). We performed quantitative real time-PCR (qRT-PCR) to determine the mRNA expression of varying Wnt signaling components and known downstream target genes in the epithelial compartment. In comparison to uninjured mouse tracheas, we observed increased mRNA expression of varying Wnt signaling components, including known canonical signaling target genes *Axin2* and *Ccnd1* (encodes Cyclin D1) (Figure 1B). *In situ* hybridization studies also demonstrated increased *Axin2* mRNA at 48hpi in the surface airway epithelium (SAE) relative to uninjured airways (Figure 1C).

We next assessed the spatiotemporal expression of Wnt/β-catenin signaling pathway components in the normal repairing airway. GSK3β, a known negative regulator of canonical signaling (Liu et al., 2002; Rubinfeld et al., 1996; Yost et al., 1996), was weakly expressed in the uninjured airway epithelium and is most strongly expressed 72hpi as proliferation declines following injury (Figure S1A). Further, β-catenin post-translational modifications (PTMs) regulate its subcellular localization and signaling in other contexts (Fang et al., 2007; Huber and Weis, 2001; Rhee et al., 2007). To determine whether β-catenin PTMs might be important in the setting of ABSC proliferation following injury, we performed IFs for several known β-catenin phosphorylation sites. We observed that β-catenin phosphorylated at tyrosine 489 (p-β-catenin^{Y489}) robustly localized to the nucleus in the repairing SAE relative to uninjured control animals (Figure 1D). This stood in contrast to other phosphorylated forms of β-catenin that primarily remained cytoplasmic or membranous (Figures S1B,C). We additionally employed *TCF/Lef:H2B/GFP* reporter mice to monitor Wnt/β-catenin pathway activity following injury *in vivo.* In contrast to uninjured airways that displayed minimal reporter activity, mice injured with polidocanol exhibited induced nuclear TCF/Lef activity that was statistically significant (Figures 1E,F). These data collectively demonstrate that the canonical Wnt/p-β-catenin^{Y489} signaling axis is activated during repair following injury *in vivo.*

To test whether β-catenin signaling was necessary for repair *in vivo,* we utilized *K5-CreER;Ctnnb1*$^{fl/fl}$ transgenic mice, a tamoxifen-inducible system that selectively deletes the β-catenin gene in K5-expressing cells. Mice were administered 75mg/kg tamoxifen intraperitoneally (i.p.) every 24 hours for five days, followed by one day of rest, to induce Cre-mediated recombination. Mice airways were then injured using i.t. polidocanol and sacrificed at 48hpi to assess ABSC proliferation (Figure 1G). Effective deletion of β-catenin was first determined by IF in tamoxifen-treated *K5-CreER;Ctnnb1*$^{fl/fl}$ mice relative to *Ctnnb1*$^{fl/fl}$ control littermate mice that lacked the *K5-CreER* transgene (Figure S1D). Further, in comparison to control airways, *K5-CreER;Ctnnb1*$^{fl/fl}$ mice tracheas displayed scant BrdU uptake and instead had an attenuated epithelium at 48hpi (Figure 1H). Taken together, these experiments illustrate that canonical Wnt/β-catenin signaling is essential for driving the proliferative phase of proximal airway regeneration following injury *in vivo.*

Porcupine-dependent phosphorylation of β-catenin at Y489 regulates ABSC proliferation

With knowledge that β-catenin is essential for proliferation in repair, we next sought to determine whether this process was regulated by upstream Wnt ligand secretion. Porcupine is an ER-resident protein known to palmitoylate all 19 mammalian Wnt ligands that is necessary for their secretion (Barrott et al., 2011; Biechele et al., 2011). As such, Porcupine plays an integral role by functioning as an upstream regulator of the Wnt signaling cascade. To determine whether Wnt secretion regulates airway epithelial proliferation after injury *in vivo*, we administered wild type mice either vehicle or small molecule Porcupine inhibitor, LGK974, prior to polidocanol-induced airway injury as shown in the schematic in Figure 2A. Relative to vehicle-treated mice, LGK974-treated mice exhibited an attenuated SAE with few BrdU+ ABSCs (Figures 2B,C), thereby phenocopying the repair response of *K5-CreER;Ctnnb1*$^{fl/fl}$ mouse tracheas. LGK974-treated mice also displayed reduced TCF/Lef:H2B/GFP reporter activity in comparison to vehicle-treated controls following injury indicating suppression of canonical Wnt signaling (Figures S2A,B). Furthermore, we observed a statistically significant decrease in the percentage of K5+ ABSCs that harbored nuclear p-β-catenin^{Y489} in mice treated with LGK974 when compared to vehicle-treated mice (Figures 2D,E). We additionally treated human ABSCs (hABSCs) *in vitro* with LGK974 and identified that those treated with Wnt secretion inhibition displayed a significant reduction in the percentage of hABSCs with nuclear p-β-catenin^{Y489} (Figures S2C,D). Taken together, these efforts indicate that Porcupine-dependent phosphorylation of β-catenin^{Y489} is necessary for ABSC proliferation.

ABSC-derived Wnt secretion is dispensable for ABSC proliferation and early progenitor cell formation following injury *in vivo.*

In light of our data that Wnt ligand secretion is necessary for the ABSC proliferative response to injury, we next sought to determine the potential cellular sources of Wnt ligand that mediate this phase of repair. To this end, we performed Porcupine IF staining in the repairing wildtype mouse airway to demarcate Wnt-producing cells within signaling niches (Tammela et al., 2017). Tracheas at 48hpi harbored Porcupine+ cells in the SAE as well as subepithelial cells in the ICZ niche, a strong upregulation in comparison to uninjured controls (Figure 3A). Additionally, the Wnt-secreting ICZ niche was dynamic and transiently activated, as 72hpi airways exhibited Porcupine expression only in the SAE and

not in cells of the ICZ (Figure 3A). These data offered two possible distinct cellular mechanisms by which Wnt-mediated proliferation occurs: one in which stem cell-derived Wnt ligand promotes proliferation or a second in which the ICZ niche provides this cue.

To dissect whether Wnt secretion from K5+ ABSCs was necessary for repair following injury, we utilized *K5-CreER;Porcn$^{fl/fl}$;ROSA$^{mT/mG}$* mice that harbor selective blockade of Porcupine and Wnt secretion in exclusively K5+ ABSCs. The repairing tracheas of these mice therefore only receive stromal paracrine Wnt contribution. We injured the *K5-CreER;Porcn$^{fl/fl}$;ROSA$^{mT/mG}$* mice and *Porcn$^{fl/fl}$;ROSA$^{mT/mG}$* control littermate mice and analyzed the repair response at varying timepoints post-injury (Figure 3B). In the absence of tamoxifen treatment, all cells have membrane-targeted tdTomato. Tamoxifen administration therefore allowed for selective Porcupine deletion in K5+ cells and triggered membrane-targeted EGFP in these cells. Effective Porcupine deletion in K5-expressing cells was first confirmed by IF. 81.97% ± 7.18% of K5+ ABSCs in *K5-CreER;Porcn$^{fl/fl}$;ROSA$^{mT/mG}$* mice underwent recombination upon tamoxifen treatment (Figures 3C,S3A). We administered polidocanol via oropharyngeal aspiration in adherence with recently published protocols (Plasschaert et al., 2018). We first identified that the repair response timeline is identical to that of mice receiving intratracheal polidocanol (data not shown). H&E staining demonstrated that the repairing airways of mouse tracheas with Porcupine deletion in K5+ ABSCs were phenotypically indistinguishable from those of control mice (Figure S3B). Assessment of BrdU incorporation from these mice at 48hpi showed no statistically significant difference (Figures 3D,E). Immunostaining analysis also identified that the 48hpi *K5-CreER;Porcn$^{fl/fl}$;ROSA$^{mT/mG}$* SAE contained uniformly GFP+ cells, indicating that the repairing airway was comprised of ABSCs devoid of Porcupine and therefore Wnt secretion (Figure S3C). Further, control *K5-CreER;ROSA$^{mT/mG}$* and experimental *K5-CreER;Porcn$^{fl/fl}$;ROSA$^{mT/mG}$* mice exhibited no differences in the formation of K8+ early progenitors at 96hpi (Figures 3F,G). Together, these results collectively demonstrate that ABSC-derived Wnt ligand is dispensable for ABSC proliferation and K8+ early progenitor formation.

The ICZ Pdgfrα+ lineage is a critical source of Wnt ligand for ABSC proliferation *in vivo.*

Our data thus far indicated that although Wnt secretion was necessary for ABSC proliferation following injury, this process was not driven by the ABSC lineage. We therefore next reasoned that the dynamic, transiently activated Wnt-secreting ICZ niche was necessary to drive ABSC proliferation following injury. To address this possibility, we administered *K5-CreER;Porcn$^{fl/fl}$;ROSA$^{mT/mG}$* mice either tamoxifen and vehicle to selectively block Wnt secretion from only the ABSC lineage, or tamoxifen and LGK974 to block global Wnt secretion prior to injury (Figure 4A). Analysis of tracheas at 48hpi illustrated that *K5-CreER;Porcn$^{fl/fl}$;ROSA$^{mT/mG}$* mice treated with LGK974 exhibited an attenuated SAE with a statistically significant decrease in the percentage of proliferating BrdU+ K5+ ABSCs in comparison to those treated with vehicle (Figures 4B,C). These data offered the insight that the Wnt-producing ICZ niche is necessary for airway epithelial proliferation following injury.

The ICZ has been speculated to serve as a signaling niche for the proximal SAE and is rich in Pdgfrα+ fibroblasts (Borthwick et al., 2001; Tadokoro et al., 2014). To further characterize the Wnt-secreting ICZ compartment during proximal airway regeneration, we utilized tamoxifen-inducible *Pdgfra-CreER;ROSA*$^{mT/mG}$ mice to label the Pdgfrα+ lineage prior to injury. We treated these mice with tamoxifen before injury, administered polidocanol, and sacrificed them at 48hpi to determine whether the Pdgfrα+ lineage in the ICZ secretes Wnt ligand during repair (Figure 4D). We first confirmed that the Pdgfrα+ cell lineage, marked by GFP, localizes to the ICZ (Figure 4E). Further lineage tracing analysis and IF staining showed that a subset of Pdgfrα+ cells in the ICZ were Porcupine+ at 48hpi (Figure 4E) while only sparse Pdgfrα+ cells were also Porcupine+ in the uninjured state (~1%) (Figure 4F). We further quantified at 48hpi that of the cells that express Porcupine and/or Pdgfrα, ~43% are Pdgfrα+ Porcupine+ cells (yellow bar graphs) (Figure 4F).

To determine whether Wnt secretion from the Pdgfrα+ lineage was necessary for proximal airway epithelial proliferation after injury, we injured *Pdgfra-CreER;Porcn*$^{fl/fl}$*;ROSA*$^{mT/mG}$ mice that will have deletion of Porcupine from the Pdgfrα+ lineage and *Pdgfra-CreER;ROSA*$^{mT/mG}$ control animals that will only have the Pdgfrα+ lineage labeled. We administered mice BrdU at 36hpi and subsequently euthanized them at 48hpi. Relative to control mice that exhibited a robust proliferative response, those with blocked Wnt secretion from the Pdgfrα+ lineage had an attenuated epithelium with a statistically significant decrease in the percentage of K5+ BrdU+ cells (Figures 4G,H). Collectively, these efforts reveal that the Pdgfrα+ ICZ niche is necessary to promote paracrine Wnt-mediated ABSC proliferation following injury.

ABSC-derived Wnt secretion is necessary for differentiation to the ciliated cell fate

Specification to the motile cilia lineage from ABSCs is regulated by cellular and molecular mechanisms distinct from those that underpin proliferation. However, Wnt/β-catenin signaling has also been implicated in mucociliary differentiation (Brechbuhl et al., 2011; Malleske et al., 2018). To monitor changes in Wnt signaling during differentiation, we stripped the SAE of uninjured mice or at 96hpi, isolated RNA, and conducted qRT-PCR for mammalian Wnt ligands. Relative to uninjured controls, we observed upregulation of mRNA for *Wnt3, Wnt5b, Wnt7a,* and *Wnt9a* and a downregulation of mRNA for *Wnt3a, Wnt5a, Wnt11,* and *Wnt16* (Figure S5A). We also probed wildtype repairing airways at 96hpi for *Axin2+* expression in K5+ ABSCs and K8+ early progenitors and observed a significant increase in the percentage of each cell population expressing *Axin2* relative to uninjured airways (Figures S5B–D), indicating a Wnt-responsive SAE during the time when differentiation occurs. These data collectively offered insight that there are appreciable changes in Wnt signaling dynamics as differentiation commences, prompting us to further mechanistically dissect this phase of regeneration.

To determine the effect of β-catenin loss in ABSCs on their capacity to differentiate to the ciliated cell fate following injury, we administered tamoxifen to *K5-CreER;ROSA*$^{mT/mG}$ or *K5-CreER;Ctnnb1*$^{fl/fl}$*;ROSA*$^{mT/mG}$ mice prior to polidocanol injury and euthanized them at 14dpi (Figure 5A). This allowed us to lineage trace the fate of K5+ ABSCs under conditions in which β-catenin was deleted from the stem cell compartment. We first observed regions

of epithelium that remained stratified in the *K5-CreER;Ctnnb1$^{fl/fl}$;ROSA$^{mT/mG}$* mice tracheas that were not present in *K5-CreER;ROSA$^{mT/mG}$* mice, consistent with a delay in returning to the normal pseudostratified mucociliary epithelium (Figure 5B, cyan box). Regions that were ciliated in the tracheas of *K5-CreER;Ctnnb1$^{fl/fl}$;ROSA$^{mT/mG}$* mice were often GFP-, indicating that they arose from a lineage that maintained β-catenin expression (Figure 5B, magenta box). We also identified a significant decrease in the percentage of GFP + lineage-traced ciliated cells that emerged at 14dpi from *K5-CreER;Ctnnb1$^{fl/fl}$;ROSA$^{mT/mG}$* mice in comparison to *K5-CreER;ROSA$^{mT/mG}$* mice (Figures 5B,C).

In light of our data indicating the necessity of β-catenin in ciliated cell differentiation *in vivo,* we next asked whether this process was mediated by an intra-epithelial Wnt-secreting niche. To answer this question, we isolated wild type mABSCs and cultured them under submerged conditions for four days. We then took the cultures to the air-liquid interface (ALI) and subsequently treated the cultures with either DMSO or LGK974 for 8 days (Figure S5E). The timing of these treatments to be only in the ALI phase of culture allowed us to isolate the effect of epithelial Wnt secretion selectively during differentiation and not proliferation. mABSC ALI cultures treated with LGK974 had a significant reduction in the percentage of differentiated ciliated cells in comparison to those treated with DMSO (Figures S5F,G). These data highlighted that an epithelial source of Wnt ligand promoted ABSC differentiation to ciliated cells. We therefore next conducted ALI experiments using mABSCs from *K5-CreER;ROSA$^{mT/mG}$* or *K5-CreER;Porcn$^{fl/fl}$;ROSA$^{mT/mG}$* to determine whether Wnt secretion from the ABSC lineage was necessary for proper ciliated cell differentiation. Cultures with ABSCs from these mice were treated *in vitro* with (Z)-4-Hydroxytamoxifen (4-OHT), the active metabolite of tamoxifen, to induce labeling of K5+ mABSCs with or without deletion of Porcupine (Figure 5D). There was a significant reduction of GFP+ and GFP- lineage-traced ciliated cells from the ALI cultures using *K5-CreER;Porcn$^{fl/fl}$;ROSA$^{mT/mG}$* mABSCs in comparison to those from *K5-CreER;ROSA$^{mT/mG}$* mABSCs (Figures 5E–G), indicating that either the K5+ ABSCs or their lineage are an important source of Wnt ligand for differentiation.

To monitor this biology *in vivo,* we administered tamoxifen to *K5-CreER;ROSA$^{mT/mG}$* or *K5-CreER;Porcn$^{fl/fl}$;ROSA$^{mT/mG}$* mice prior to polidocanol injury and euthanized them at 9dpi (Figure 5H). While we observed no statistically significant difference between the percentage of GFP+ lineage-traced ciliated cells between the two transgenic mouse models (Figures 5I,J), we qualitatively appreciated that the acetylated β-tubulin immunostaining in the GFP+ lineage in the *K5-CreER;Porcn$^{fl/fl}$;ROSA$^{mT/mG}$* mice was fainter and the microtubules appeared shorter on confocal microscopy (Figure 5I). Strikingly, analysis by transmission electron microscopy identified that while wildtype mice contained mature cilia on the surface of all ciliated cells, those with deletion of Porcupine in the K5+ lineage showed about 31.5% of the ciliated cells had shortened and sparse cilia (Figures 5K,L), indicating a delay or defect in motile ciliogenesis. Overall, we saw an induction in the percentage of multi-ciliated cells that harbored immature cilia in the tracheas of *K5-CreER;Porcn$^{fl/fl}$;ROSA$^{mT/mG}$* mice relative to *K5-CreER;ROSA$^{mT/mG}$* mice (Figure 5L). Further, cross-sections through the apical surface of wildtype cells showed basal bodies that were fully docked to the apical surface, while many mutant cells contained basal bodies that

were localized throughout the cytoplasm (Figure 5K). These data allowed us to confirm that an intra-epithelial source of Wnt ligand is necessary for proper differentiation to the motile ciliated cell fate.

Because perturbations in transgenic mouse models using the *K5-CreER* tissue-specific driver affects ABSCs and their entire lineage, we sought to assay whether the K8+ early progenitor cell may be a key cell type that allows for Wnt-mediated ciliated cell differentiation. To address this possibility, we conducted ALI experiments using mABSCs from *K8-CreER;ROSA*$^{mT/mG}$ or *K8-CreER;Porcn*$^{fl/fl}$*;ROSA*$^{mT/mG}$ to determine if Wnt secretion from the K8+ early progenitor cell was necessary for ABSC differentiation to the ciliated cell. (Figure S5H). Interestingly, we observed no statistically significant difference in the percentage of GFP+ or GFP- ciliated cells that arose in ALI between the two transgenic mice (Figures S5I–K), suggesting that Wnt secretion from the K8+ cell is dispensable for differentiation. Taken together, our data suggest that Wnt secretion from the K5+ ABSC signals to the K8+ early progenitor that facilitates differentiation to the ciliated cell fate, underscoring the emergence of an intra-epithelial Wnt niche during this phase of repair.

Glandular-like epithelial invaginations (GLEIs) emerge exclusively in the ICZ during aging, arise from ABSCs, and contribute to homeostasis and repair

The molecular and cellular mechanisms that govern homeostasis and repair are known to become dysregulated during aging and are linked with disease progression (Biteau et al., 2008; Cosgrove et al., 2014; Merlos-Suarez et al., 2011). As such, we sought to understand how the proximal airway stem cell niche changes across the aging spectrum. Previous work has begun to note changes in the mouse proximal airway morphology during the aging process (Nettesheim and Martin, 1970; Wansleeben et al., 2014). Consistent with this, we observed the previously reported age-related gland-like structures in distal trachea of 12-month-old-mice, herein referred to as glandular-like epithelial invaginations (GLEIs). Interestingly, however, GLEIs localized exclusively in the ICZ and harbored ducts that connect to the SAE and were not present in young mouse airways (Figure 6A). These structures bear morphologic resemblance to submucosal glands that are located only in the most proximal portion of the mouse trachea (Wine and Joo, 2004)(Figure 6A). GLEIs contain K5+ ABSCs (Figure 6B) as well as ciliated and mucus-producing cells by IF and Alcian Blue Periodic Acid-Schiff staining, respectively (Figures S6A,B), but have neither branching tubules nor myoepithelial cells (Wansleeben et al., 2014). We additionally performed IF staining on 24-month-old tracheas and identified that GLEIs and their connective ducts are contained by a defined basement membrane, as determined by laminin staining (Figure 6C), indicating that these structures are contiguous with the SAE.

To further characterize the aging trachea, we performed IFs on tracheas from mice at 7 weeks, 12 months, and 24 months of age for K5 and acetylated β-tubulin (Figure 6D). We first appreciated a stark decrease in the percentage of K5+ ABSCs in the SAE during the aging process (Figures 6D,E). However, when the percentage of K5+ ABSCs from the SAE and GLEIs were combined, we observed no statistically significant difference between the number of total ABSCs from mice at 7 weeks, 12 months, and 24 months of age (Figure 6F).

Of note, there was also no difference in the percentage of ciliated cells during aging as measured by acetylated β-tubulin immunostaining (Figure S6C).

To understand the potential function of GLEIs, we first administered a 12-hour BrdU pulse *in vivo* to 12-month old mice. We observed that K5+ ABSCs of GLEIs preferentially uptake BrdU label in comparison to those in the SAE, suggesting that GLEIs likely contribute to proximal airway turnover and homeostasis (Figure 6G). Further, ABSCs in GLEIs were proliferative post-polidocanol injury, as evidenced by BrdU incorporation at 48hpi, indicating their contribution to repair (Figure 6H). We next sought to determine the cellular origin of GLEIs. To address this question, we labeled the K5+ ABSCs of *K5-CreER;ROSA*$^{mT/mG}$ mice at 1.5 months of age by administering tamoxifen to them at this time (Figure 6I). We then aged these mice to 12 months and observed that GLEIs contained the GFP+ lineage trace (Figure 6J), suggesting that K5+ ABSCs labeled during youth migrate into the ICZ to form GLEIs during aging. Together, we identified GLEI structures that are contained by a basement membrane and contiguous with the SAE, are of K5+ origin, and contribute to proximal airway homeostasis and repair.

A dynamic ABSC Wnt-secreting niche facilitates GLEI formation during aging *in vivo.*

We next inquired whether Wnt signaling within the proximal airway stem cell niche changes during aging. To assess the extent of Wnt secretion during tracheal aging, we performed IF staining for Porcupine on aged mouse tracheas. We identified that a subset of SAE ABSCs, GLEI ABSCs, and cells in the ICZ were marked by Porcupine expression in the uninjured and injured states (Figure 7A). These findings stood in contrast to young airways with no Porcupine expression at baseline (Figure 3A), thereby indicating a primed, actively signaling niche at baseline. We profiled how expression of the known mammalian Wnt ligands changes during aging and observed a strong upregulation of Wnt2 and downregulation of Wnt7a mRNA as measured by qRT-PCR (Figure 7B), indicating notable dynamic changes in Wnt signaling during aging.

Our data highlighting changes in Wnt activity in aging offered the possibility that Wnt may regulate proximal airway aging phenotypes. Further, Wansleeben et al. demonstrated that TCF/LEF was expressed at the leading edge of GLEIs (Wansleeben et al., 2014), suggesting that Wnt/β-catenin signaling may be important in their formation. To determine whether the aging morphologic changes can be attributed to Wnt signaling, we first employed *K5-CreER;Ctnnb1*$^{LSL(Ex)/+}$*;ROSA*$^{mT/mG}$ mice, which selectively delete the third exon of the gene encoding β-catenin in K5-expressing cells upon tamoxifen administration. Deletion of this exon produces a form of β-catenin that escapes proteasomal degradation and remains constitutively active (Harada et al., 1999). *K5-CreER;Ctnnb1*$^{LSL(Ex)/+}$*;ROSA*$^{mT/mG}$ or *K5-CreER;ROSA*$^{mT/mG}$ mice were treated with tamoxifen at 7-weeks of age for 5 days followed by euthanasia on day 12 (Figure 7C). Lineage tracing studies demonstrated that constitutively active β-catenin in K5+ ABSCs was sufficient to promote occasional GLEI formation in young mice (Figure 7D). Further, mABSCs cultured in matrigel *in vitro* from *K5-CreER;Ctnnb1*$^{LSL(Ex)/+}$*;ROSA*$^{mT/mG}$ mice demonstrated the emergence of spheres that had tongue-like protrusions in comparison to tracheospheres from *K5-CreER;ROSA*$^{mT/mG}$ mice (Figure 7E), recapitulating a phenotype mirroring that of mouse tracheas *in vivo.*

While our present studies have identified that ectopic activation of β-catenin in K5+ ABSCs was sufficient for GLEI formation, we next asked which cell types were necessary for their formation during aging. To this end, we administered tamoxifen to *Porcn*$^{fl/fl}$ control mice or *K5-CreER;Porcn*$^{fl/fl}$ mice at 1.5 months of age and allowed them to age to 7 months (Figure 7F). *K5-CreER;Porcn*$^{fl/fl}$ mice harbored significantly fewer GLEIs in the ICZ in comparison to *Porcn*$^{fl/fl}$ mice at 7 months of age (Figures 7G,H). Taken together, these data highlight the spatiotemporal dynamism of Wnt signaling in the aged proximal airway, as ABSC-derived Wnt ligand is necessary for GLEI formation.

DISCUSSION

While our current understanding of Wnt signaling in mucociliary epithelia remains controversial, our efforts here elucidate its dynamic role in proximal airway regeneration and aging. We have defined functionally distinct, spatiotemporally dynamic proximal airway stem cell niches driven by Wnt signaling that together orchestrate the stem cell repair response as well as changes in aging. Under homeostatic conditions in youth, the proximal airway exhibits little Wnt signaling. During injury repair, however, cells marked by the Pdgfrα+ lineage in the ICZ niche are an important source of Wnts that promote tracheal epithelial proliferation. Interestingly, however, we observed an important dynamic cell type switch during the differentiation phase of repair accompanied by an increase in K8+ *Axin2+* cells that are apposed to K5+ ABSCs. Wnt secretion from the K5+ ABSCs promotes the emergence of ciliated cells in the airway, underscoring a critical paracrine Wnt mechanism that drives the differentiation phase of repair. Moreover, during aging, GLEIs that are contiguous with SAE form in the ICZ and contribute to repair following injury and these structures are necessarily formed by continuous Wnt ligand secretion derived from the ABSC compartment – a cell type that secretes Wnt ligands that are dispensable for ABSC proliferation in youth.

β-catenin was shown to promote basal cell proliferation after naphthalene injury (Hsu et al., 2014). Additionally, a recent study offered a model that high levels of Wnt/β-catenin signaling activate ΔN-TP63 expression to promote basal cell proliferation (Haas et al., 2019). Two prior *in vitro* studies delineated distinctions between ABSC fate specification versus commitment to the ciliated cell fate (Brechbuhl et al., 2011; Malleske et al., 2018). Under submerged and air-liquid interface conditions *in vitro,* the proposed working model was that β-catenin is active in the late proliferation stage and during ciliated cell differentiation. These findings are consistent with others who have revealed Wnt signaling regulates expression and activity of Foxjl to promote ciliogenesis (Caron et al., 2012; Walentek et al., 2015; Walentek et al., 2012). Our work further builds upon their framework by highlighting the exquisite dynamism of critically important Wnt-secreting cell types that selectively drive not only this proliferative phase of repair, but also its functionally distinct role in differentiation and in aging. We identify distinct spatiotemporally dynamic Wnt-secreting niches that are important in distinct biological processes.

Wnt signaling plays an integral role in bronchiolar and alveolar biology. Zepp et al. recently identified and characterized five distinct mesenchymal lineages in the distal airway, one of which was a Wnt-responsive (Axin2+) Pdgfrα+ population located in proximity to alveolar

type II cells (AT2) to facilitate their differentiation to type I cells (Zepp et al., 2017). Nabhan et al., in contrast, highlighted a single Wnt-producing fibroblast that serves as a signaling niche to an adjacent AT2 cell (Nabhan et al., 2018). Another group identified alveolar Lgr5+ and bronchiolar Lgr6+ mesenchymal populations that are Wnt-producing and Wnt-responsive, respectively (Lee et al., 2017). Here, we report that cell-autonomous Wnt signaling from the K5+ airway basal stem cell is dispensable for epithelial proliferation and instead responds to Wnts produced by a dynamic Pdgfrα+ ICZ lineage that is transiently activated following injury. Our data therefore speak to critically important regional and contextual distinctions in the regenerating murine airway. Our work extends the body of efforts to dissect the nuanced mechanisms underpinning Wnt-mediated airway regeneration. It is important to note that other signaling cascades have been identified as critical regulators of ABSC self-renewal and differentiation in the adult trachea, including Notch and BMP (Paul et al., 2014; Rock et al., 2011; Tadokoro et al., 2016). Further, a recent paper analyzing the developing trachea showed that epithelial Wnt production signals to the mesenchyme, where β-catenin crosstalks with Fgf10 to, in turn, promote basal cell specification (Hou et al., 2019). Together, these and our work highlight the importance of paracrine interactions between the airway epithelium and mesenchyme.

To our knowledge, mechanisms for alterations in the proximal airway stem cell niche seen during the aging process are unexplored. Prior studies identified the emergence of age-related gland-like structures (ARGLS) during tracheal aging in the ICZ (Nettesheim and Martin, 1970; Wansleeben et al., 2014). Wansleeben et al. also identified that the distal tips of the ARGLS had nuclear TCF/LEF, as measured by reporter mice. Our work complements and further extends these efforts by identifying that ARGLS more closely resemble tracheal epithelial continuations that invaginate into the ICZ and we therefore named them glandular-like epithelial invaginations (GLEIs). GLEIs are contiguous with the SAE, are proliferative post-injury, and bear a striking structural resemblance to submucosal gland ducts. We speculate that GLEIs may represent a primitive form of submucosal gland ducts and act as a stem cell pool to contribute to local epithelial repair, similar to myoepithelial cells lining submucosal glands that act as reserve stem cells following severe injury (Hegab et al., 2011; Lynch et al., 2018; Tata et al., 2018). Our efforts also demonstrate that Wnt ligands are secreted in the uninjured aged airway, thereby further emphasizing the dynamic character of the niche. Further, the similarity between the morphology of the GLEIs and the structures in young mice with hyperactive β-catenin in K5+ ABSCs suggests that Wnt gradients in the ICZ and overlying SAE may play a role in the glandular hypertrophy previously appreciated during aging (Hernandez et al., 1965). Our efforts also revealed that GLEIs arise from K5+ ABSCs that are labeled during youth, suggesting ABSC migration during aging. The movement of K5-expressing ABSCs towards the ICZ in these areas is reminiscent of the movement of K5-expressing cells during submucosal gland development (May and Tucker, 2015). We speculate that ABSCs become more migratory during aging, which facilitates GLEI formation, and may have implications for carcinogenesis.

Our work highlights the spatiotemporally dynamic character of Wnt-producing proximal airway stem cell niches that coordinate distinct biological processes: proliferation, differentiation, and aging. Our work is consistent with findings that identify mesenchymal cells as crucial sources of Wnt and R-spondin in the developing intestinal epithelium

(Greicius et al., 2018) and therefore provides insight for biology that may be generalizable across multiple epithelial tissue types. This study illuminates the crucial need to dissect the relative contributions of epithelial and mesenchymal compartments in the context of cellular niches as well as their dynamic changes following injury. Our work further underscores the merit in segmenting these respective contributions during distinct repair phases. We believe achieving this extent of granularity in our knowledge base will allow for treatment advancements in regenerative medicine.

Limitations of the Study

We acknowledge that our study may not fully characterize the entire complexity by which the dynamic Wnt signaling niche modulates airway regeneration and aging, as there are PDGFRα positive and negative Wnt-producing cell types in the ICZ. We also appreciate that our studies did not identify the Wnt ligands responsible for signaling in each of these dynamic niches. It is likely that different Wnt ligands play different roles during the repair process, but we were not able to assess this and this could be characterized in future studies. Further, our experiments did not examine non-canonical Wnt signaling and how this may interact with canonical Wnt signaling and contribute to the airway repair process. Our study also does not consider potential nodes of crosstalk with other signaling pathways, including the Notch and PI3K/Akt signaling pathways. It seems likely that these signaling pathways interact with one another and further studies are needed to understand how they are connected to orchestrate the stem cell repair response. Our data were almost exclusively obtained in transgenic mouse models and whether our observations of Wnt signaling dynamics for airway repair and aging will translate to humans will require patient samples obtained after airway injury and airway samples obtained throughout the lifespan.

STAR METHODS

RESOURCE AVAILABILITY

Lead contact—Further information and requests for resources and reagents should be directed to and will be fulfilled by the Lead Contact, Brigitte N. Gomperts (BGomperts@mednet.ucla.edu).

Materials Availability—This study did not generate new unique reagents.

Data and Code Availability—This study did not generate/analyze datasets/codes.

Method Details

Mice—All animal experiments were approved by the Animal Research Committee at UCLA. 6–10-week-old male and female C57BL/6J wild type mice were purchased from The Jackson Laboratory (Bar Harbor, Maine). *K5-CreER*^{T2} mice, *K8-CreER*^{T2} mice, *ROSA*$^{mT/mG}$ mice, *Porcn*$^{fl/fl}$ mice, *Pdgfrα-CreER*^{TM} mice, *TCF/Lef:H2B/GFP* mice, and *Ctnnb1*$^{fl/fl}$ mice were all obtained from The Jackson Laboratory. *Ctnnb1*$^{LSL(Ex3)/+}$ mice were a generous gift from Dr. Mark Taketo via Dr. Bart Williams at the Van Andel Institute. Mice were maintained in a pathogen-free facility at the Division of Laboratory Animal Medicine (DLAM) at UCLA. Transgenic mice were genotyped by PCR after genomic DNA

isolation of ear biopsies following protocols by The Jackson Laboratory. Genotyping primers and PCR conditions are shown in Table S1 and Table S2, respectively. All young experiments used either WT or age-matched transgenic mice at 6–10 weeks old. All wild type mouse aging experiments used 12- to 24-month-old mice. To induce recombination in transgenic mice, 75mg/kg tamoxifen was administered i.p. every 24 hours for 5 days followed by 1 day of rest.

Mouse Ear Genomic DNA Isolation—Clipped ears were incubated in 100μL of 0.05M NaOH at 100°C for 20 minutes. Samples then received 8.3μl of 1M Tris-HCl, pH 8.5 and vortexed. 1μL genomic DNA was used per genotyping PCR reaction.

Human Tissue Procurement—Large airways and bronchial tissues were acquired from de-identified normal human donors after lung transplantations at the Ronald Reagan UCLA Medical Center. Tissues were procured under Institutional Review Board-approved protocols at the David Geffen School of Medicine at UCLA.

ABSC Isolation and Fluorescence-Activated Cell Sorting (FACS)—Mouse and human ABSCs were isolated following a previously published method by our laboratory (Hegab et al., 2012a; Hegab et al., 2014; Hegab et al., 2012b; Paul et al., 2014). Briefly, mouse tracheas were dissected, cleaned, and incubated in 16U/mL dispase for 30 minutes at room temperature. Tracheas were then incubated in 0.5mg/mL DNase for another 30 minutes at room temperature. Epithelium was stripped and incubated in 0.1% Trypsin-EDTA for 30 minutes shaking at 37°C to generate a single cell suspension. Isolated cells were passed through a 40μm strainer and stained with fluorophore-conjugated antibodies against ITGA6 and TROP2. ITGA6+ TROP2+ cells were obtained via FACS that was completed using the BD FACSAria cell sorter.

Air-Liquid Interface (ALI) Cultures and *In Vitro* Treatments—24-well 6.5mm transwells with 0.4μm pore polyester membrane inserts were coated with 0.2mg/mL collagen type I dissolved in 60% ethanol and allowed to air dry. ABSCs were seeded at 100,000 cells per well in a 1:1 mixture of media:growth factor-reduced Matrigel to grow as tracheospheres or seeded directly onto collagen-coated transwells and allowed to grow in the submerged phase of culture for 4–5 days with 500μl media in the basal chamber and 200μl media in the apical chamber. ALI cultures were then established and cultured with only 500μl media in the basal chamber, and cultures were harvested at varying timepoints for IF studies. Media was changed every other day and cultures were maintained at 37°C and 5% CO_2. ABSCs were treated with the indicated concentrations of LGK974 or 4-OHT.

Mouse Tracheal Epithelial Cell (MTEC) Plus and Serum-Free Media—Mouse ABSCs were grown in MTEC Plus media and MTEC serum-free media during the submerged and ALI phases of culture, respectively. MTEC base media is DMEM/Ham's F12 50/50 (Corning 15090CV). Table S3 and Table S4 indicate the media components and concentrations for MTEC Plus and MTEC serum-free media, respectively.

Polidocanol Airway Injury and *In Vivo* Treatments—Proximal mouse airway epithelium was injured with polidocanol following previously published protocols

(Borthwick et al., 2001; Paul et al., 2014). Briefly, 6–10-week-old male and female WT or transgenic mice received 100μL 0.6mg/mL carprofen and were anesthetized using 3% vaporized isoflurane. Freshly prepared 2% polidocanol was diluted in PBS. For intratracheal instillation of polidocanol, mice were placed supine for the duration of the procedure and 10μL injected using a BD Insulin Syringe M/Fine 0.3mL (31G). For oropharyngeal aspiration delivery of polidocanol, mice were placed upright on an intubation board at an approximately 70° angle, hanging teeth along string in adherence with previously published protocols (Plasschaert et al., 2018). Nose pinchers were used to close nostrils and ensure the mouse was breathing by mouth. 18μL of polidocanol was then pipetted to back of the mouth and the mouse was allowed to aspirate. Mice were euthanized at various timepoints post-injury and tracheas were removed, fixed in 4% paraformaldehyde overnight, incubated overnight in 20% sucrose, and subsequently embedded in paraffin or OCT for sectioning and immunofluorescence.

For *in vivo* pharmacologic inhibition of Porcupine, mice were treated with vehicle (10% DMSO, 90% corn oil) or 10mg/kg LGK974 dissolved in vehicle several days prior to polidocanol injection, day of polidocanol injection, and every 48 hours post-injury. For *in vivo* proliferation studies, mice were injected intraperitoneally with 50mg/kg BrdU 12 hours prior to euthanasia to label cells in S-phase. The percentage of dividing cells (BrdU+/DAPI +) was calculated as previously described (Paul et al., 2014).

Immunocytochemistry—Mouse and human ABSCs were fixed in 4% paraformaldehyde for 15 minutes followed by permeabilization with 0.5% Triton-X for 10 minutes. Cells were then blocked using serum-free protein block (Dako X090930) for one hour at room temperature and overnight primary antibody incubation. After several washes of Tris-Buffered Saline and Tween-20 (TBST), secondary antibodies were incubated on samples for 1 hour in darkness, washed, and mounted using Vectashield hardest mounting medium with DAPI (Vector Labs H-1500). IF images were obtained using an LSM780 or LSM880 Zeiss confocal microscope and composite images generated using Fiji. The list of antibodies used is provided in the Key Resources Table as part of STAR Methods.

Immunofluorescence (IF)—4–5μm thick paraffin-embedded sections were deparaffinized by placing them on a 60°C heating block for 1–2 hours and through a series of Histo-Clear and ethanol washes. Antigen retrieval was then performed using a pressure cooker for 10 minutes in 1mM EDTA or 10mM Citrate Buffer, pH 6.0. Samples were then permeabilized with 0.5% Triton-X and blocked using serum-free protein block (Dako X090930) for one hour at room temperature and overnight primary antibody incubation. After several washes of TBST, secondary antibodies were incubated on samples for 1 hour in darkness, washed, and mounted using Vectashield hardest mounting medium with DAPI (Vector Labs H-1500). IF images were obtained using an LSM780 or LSM880 Zeiss confocal microscope and composite images generated using Fiji. The list of antibodies used is provided in the Key Resources Table as part of the STAR Methods.

Quantitative Polymerase Chain Reaction (qPCR)—RNA was isolated with the RNeasy Mini Kit (Qiagen 74104) following manufacturer's protocol and quantified using a NanoDrop Spectrophotometer (ThermoFisher). cDNA synthesis was performed using the

TaqMan Reverse Transcription Reagents (ThermoFisher) or iScript cDNA Synthesis Kit (BioRad)s as indicated by the respective company. qPCR was then performed using the TaqMan PCR Master Mix (Applied Biosystems) or using the Mouse Wnt Signaling Pathway RT^2 Profiler PCR Array (Qiagen) on the StepOne-Plus Real Time PCR System. Samples were run in triplicate for studies outside of the profiler array and fold changes in expression were determined using the comparative DC_T method and 18S rRNA as an endogenous control. TaqMan Probes used are listed in Table S5.

RNA *In Situ* Hybridization—RNAScope technology (ACD Bio) was used to perform RNA *in situ* hybridization (RNA ISH) experiments (Wang et al., 2012) according to manufacturer's instructions, with the *Axin2* (400331) probe used. IF images were acquired using an automated TiE inverted fluorescence microscope platform equipped with an encoded motorized stage and Plan Apo 60× 1.40 NA objective (Nikon Instruments, Inc.). The Nikon TiE inverted fluorescence confocal microscope was outfitted with a Yokogawa X1 spinning disk head and Andor DU-897 EM-CCD. Lasers utilized for excitation included 405, 488, 561, and 647nm, and emission filters were 455/50, 525/36, 641/75, and 700/74 (peak/bandwidth), respectively. NIS-Elements software (Nikon Instruments, Inc.) was utilized for image acquisition.

Proximity Ligation *In Situ* Hybridization (PLISH)—PLISH was performed in adherence to previously published protocols (Nagendran et al., 2018). 4–5μm paraffin-embedded tracheal sections were hybridized with anti-sense probe pairs. Probe sequences targeting *Axin2* are listed below:

mmHRC2-VB1-Axin2–2955: 5' gtttcattttccttcagaatTTATAGGTCGAGTAGTATAGCCAGGTT 3'

mmHLC2-VB1-Axin2–2955: 5' AGGTCAGGAATACTTACGTCGTTATGGatttcgtggctgttgcgtag 3'

mmHRC2-VB1-Axin2–2411: 5' cctgcggcaggcttcctctTTATAGGTCGAGTAGTATAGCCAGGTT 3'

mmHLC2-VB1-Axin2–2411: 5' AGGTCAGGAATACTTACGTCGTTATGGagctgtgccaaagtgttggg 3'

mmHRC2-VB1-Axin2–1876: 5' gacagcgtggtggtggatgtTTATAGGTCGAGTAGTATAGCCAGGTT 3'

mmHLC2-VB1-Axin2–1876: 5' AGGTCAGGAATACTTACGTCGTTATGGagtggtggtgaacgtgcttc 3'

mmHRC2-VB1-Axin2–347: 5' gatctggaaggagagtcactTTATAGGTCGAGTAGTATAGCCAGGTT 3'

mmHLC2-VB1-Axin2–347: 5' AGGTCAGGAATACTTACGTCGTTATGGaacacggcgctactcatggt 3'

Transmission Electron Microscopy—Tissues were fixed in 2% glutaraldehyde, 4% paraformaldehyde in 0.1M NaCocodylate buffer, pH 7.4 at 4°C overnight. Samples were osmicated, stained with uranyl acetate, then dehydrated with a graded ethanol series and infiltrated with Embed-812 (Electron Microscopy Sciences). 80nm sections were mounted onto copper grids and analyzed with an FEI Tecnai G2 transmission electron microscope (Hillsboro, OR) with an AMT side-mount digital camera (Woburn, MA).

Statistical Analysis—Data are presented as the mean ± standard error of the mean (SEM) values. Student's t-tests were used to assess statistical significance. Calculated p-values are indicated on individual figures. *$p < 0.05$, **$p < 0.01$, ***$p < 0.001$, n.s. = not significant.

Supplementary Material

Refer to Web version on PubMed Central for supplementary material.

ACKNOWLEDGMENTS

This work was supported by the UCLA Medical Scientist Training Program grant (NIH NIGMS GM008042) (CA), the NIH/NCI NRSA Predoctoral F31 Diversity Fellowship F31CA239655 (CA), the UCLA Eli & Edythe Broad Center of Regenerative (BSCRC) Medicine and Stem Cell Research Training Grant (CA), the T32 National Research Service Award in Tumor Cell Biology CA009056 (CA), the NIH/NCI Grant R01CA208303 (BG), the Tobacco Related Disease Research Program (TRDRP) High Impact Pilot Research Award (HIPRA) 26IP-0036 (BG), the TRDRP HIPRA 29IP-0597 (BG), The UCLA Jonsson Comprehensive Cancer Center, (JCCC) STOP Cancer Award (BG), the Ablon Research Scholars Award (BG), and the UCLA Maximizing Student Development Award NIH NIGMS R25GM055052 (CP). We appreciate the UCLA BSCRC Microscopy and Flow Cytometry Cores and the JCCC Flow Cytometry Core. We also thank and Dr. Mark Taketo at Kyoto University via Dr. Bart Williams from the van Andel Institute for generously sending us hyperactive β-catenin mice Statistical analyses were supported by the NIH/National Center for Advancing Translational Science (NCATS) UCLA CTSI Grant Number UL1TR000124.

REFERENCES

Barkauskas CE, Cronce MJ, Rackley CR, Bowie EJ, Keene DR, Stripp BR, Randell SH, Noble PW, and Hogan BL (2013). Type 2 alveolar cells are stem cells in adult lung. J Clin Invest 123, 3025–3036. [PubMed: 23921127]

Barrott JJ, Cash GM, Smith AP, Barrow JR, and Murtaugh LC (2011). Deletion of mouse Porcn blocks Wnt ligand secretion and reveals an ectodermal etiology of human focal dermal hypoplasia/Goltz syndrome. Proc Natl Acad Sci U S A 108, 12752–12757. [PubMed: 21768372]

Biechele S, Cox BJ, and Rossant J (2011). Porcupine homolog is required for canonical Wnt signaling and gastrulation in mouse embryos. Dev Biol 355, 275–285. [PubMed: 21554866]

Biteau B, Hochmuth CE, and Jasper H (2008). JNK activity in somatic stem cells causes loss of tissue homeostasis in the aging Drosophila gut. Cell Stem Cell 3, 442–455. [PubMed: 18940735]

Borthwick DW, Shahbazian M, Krantz QT, Dorin JR, and Randell SH (2001). Evidence for stem-cell niches in the tracheal epithelium. Am J Respir Cell Mol Biol 24, 662–670. [PubMed: 11415930]

Brechbuhl HM, Ghosh M, Smith MK, Smith RW, Li B, Hicks DA, Cole BB, Reynolds PR, and Reynolds SD (2011). beta-catenin dosage is a critical determinant of tracheal basal cell fate determination. Am J Pathol 179, 367–379. [PubMed: 21703416]

Caron A, Xu X, and Lin X (2012). Wnt/beta-catenin signaling directly regulates Foxj1 expression and ciliogenesis in zebrafish Kupffer's vesicle. Development 139, 514–524. [PubMed: 22190638]

Cole BB, Smith RW, Jenkins KM, Graham BB, Reynolds PR, and Reynolds SD (2010). Tracheal Basal cells: a facultative progenitor cell pool. Am J Pathol 177, 362–376. [PubMed: 20522644]

Cosgrove BD, Gilbert PM, Porpiglia E, Mourkioti F, Lee SP, Corbel SY, Llewellyn ME, Delp SL, and Blau HM (2014). Rejuvenation of the muscle stem cell population restores strength to injured aged muscles. Nature medicine 20, 255–264.

Desai TJ, Brownfield DG, and Krasnow MA (2014). Alveolar progenitor and stem cells in lung development, renewal and cancer. Nature 507, 190–194. [PubMed: 24499815]

Donne ML, Lechner AJ, and Rock JR (2015). Evidence for lung epithelial stem cell niches. BMC Dev Biol 15, 32. [PubMed: 26376663]

Fang D, Hawke D, Zheng Y, Xia Y, Meisenhelder J, Nika H, Mills GB, Kobayashi R, Hunter T, and Lu Z (2007). Phosphorylation of beta-catenin by AKT promotes beta-catenin transcriptional activity. J Biol Chem 282, 11221–11229. [PubMed: 17287208]

Giangreco A, Lu L, Vickers C, Teixeira VH, Groot KR, Butler CR, Ilieva EV, George PJ, Nicholson AG, Sage EK, et al. (2012). beta-Catenin determines upper airway progenitor cell fate and preinvasive squamous lung cancer progression by modulating epithelial-mesenchymal transition. J Pathol 226, 575–587. [PubMed: 22081448]

Greicius G, Kabiri Z, Sigmundsson K, Liang C, Bunte R, Singh MK, and Virshup DM (2018). PDGFRalpha(+) pericryptal stromal cells are the critical source of Wnts and RSPO3 for murine intestinal stem cells in vivo. Proc Natl Acad Sci U S A 115, E3173–E3181. [PubMed: 29559533]

Haas M, Gomez Vazquez JL, Sun DI, Tran HT, Brislinger M, Tasca A, Shomroni O, Vleminckx K, and Walentek P (2019). DeltaN-Tp63 Mediates Wnt/beta-Catenin-Induced Inhibition of Differentiation in Basal Stem Cells of Mucociliary Epithelia. Cell Rep 28, 3338–3352.e3336. [PubMed: 31553905]

Harada N, Tamai Y, Ishikawa T, Sauer B, Takaku K, Oshima M, and Taketo MM (1999). Intestinal polyposis in mice with a dominant stable mutation of the beta-catenin gene. The EMBO journal 18, 5931–5942. [PubMed: 10545105]

Hegab AE, Ha VL, Attiga YS, Nickerson DW, and Gomperts BN (2012a). Isolation of basal cells and submucosal gland duct cells from mouse trachea. J Vis Exp, e3731. [PubMed: 23007468]

Hegab AE, Ha VL, Bisht B, Darmawan DO, Ooi AT, Zhang KX, Paul MK, Kim YS, Gilbert JL, Attiga YS, et al. (2014). Aldehyde dehydrogenase activity enriches for proximal airway basal stem cells and promotes their proliferation. Stem Cells Dev 23, 664–675. [PubMed: 24171691]

Hegab AE, Ha VL, Darmawan DO, Gilbert JL, Ooi AT, Attiga YS, Bisht B, Nickerson DW, and Gomperts BN (2012b). Isolation and in vitro characterization of basal and submucosal gland duct stem/progenitor cells from human proximal airways. Stem Cells Transl Med 1, 719–724. [PubMed: 23197663]

Hegab AE, Ha VL, Gilbert JL, Zhang KX, Malkoski SP, Chon AT, Darmawan DO, Bisht B, Ooi AT, Pellegrini M, et al. (2011). Novel stem/progenitor cell population from murine tracheal submucosal gland ducts with multipotent regenerative potential. Stem Cells 29, 1283–1293. [PubMed: 21710468]

Hernandez JA, Anderson AE Jr., Holmes WL, Morrone N, and Foraker AG (1965). The Bronchial Glands in Aging. J Am Geriatr Soc 13, 799–804. [PubMed: 14341027]

Hogan BL, Barkauskas CE, Chapman HA, Epstein JA, Jain R, Hsia CC, Niklason L, Calle E, Le A, Randell SH, et al. (2014). Repair and regeneration of the respiratory system: complexity, plasticity, and mechanisms of lung stem cell function. Cell Stem Cell 15, 123–138. [PubMed: 25105578]

Hong KU, Reynolds SD, Watkins S, Fuchs E, and Stripp BR (2004). Basal cells are a multipotent progenitor capable of renewing the bronchial epithelium. Am J Pathol 164, 577–588. [PubMed: 14742263]

Hou Z, Wu Q, Sun X, Chen H, Li Y, Zhang Y, Mori M, Yang Y, Que J, and Jiang M (2019). Wnt/Fgf crosstalk is required for the specification of basal cells in the mouse trachea. Development 146.

Hsu HS, Liu CC, Lin JH, Hsu TW, Su K, and Hung SC (2014). Repair of naphthalene-induced acute tracheal injury by basal cells depends on beta-catenin. J Thorac Cardiovasc Surg 148, 322–332. [PubMed: 24280717]

Huber AH, and Weis WI (2001). The structure of the beta-catenin/E-cadherin complex and the molecular basis of diverse ligand recognition by beta-catenin. Cell 105, 391–402. [PubMed: 11348595]

Kim CF, Jackson EL, Woolfenden AE, Lawrence S, Babar I, Vogel S, Crowley D, Bronson RT, and Jacks T (2005). Identification of bronchioalveolar stem cells in normal lung and lung cancer. Cell 121, 823–835. [PubMed: 15960971]

Lee JH, Tammela T, Hofree M, Choi J, Marjanovic ND, Han S, Canner D, Wu K, Paschini M, Bhang DH, et al. (2017). Anatomically and Functionally Distinct Lung Mesenchymal Populations Marked by Lgr5 and Lgr6. Cell 170, 1149–1163 e1112. [PubMed: 28886383]

Liu C, Li Y, Semenov M, Han C, Baeg GH, Tan Y, Zhang Z, Lin X, and He X (2002). Control of beta-catenin phosphorylation/degradation by a dual-kinase mechanism. Cell 108, 837–847. [PubMed: 11955436]

Lynch TJ, Anderson PJ, Rotti PG, Tyler SR, Crooke AK, Choi SH, Montoro DT, Silverman CL, Shahin W, Zhao R, et al. (2018). Submucosal Gland Myoepithelial Cells Are Reserve Stem Cells That Can Regenerate Mouse Tracheal Epithelium. Cell Stem Cell 22, 779.

Malleske DT, Hayes D Jr., Lallier SW, Hill CL, and Reynolds SD (2018). Regulation of Human Airway Epithelial Tissue Stem Cell Differentiation by beta-Catenin, P300, and CBP. Stem Cells.

May A, and Tucker A (2015). Understanding the development of the respiratory glands. Developmental dynamics : an official publication of the American Association of Anatomists 244, 525–539. [PubMed: 25648514]

Merlos-Suarez A, Barriga FM, Jung P, Iglesias M, Cespedes MV, Rossell D, Sevillano M, Hernando-Momblona X, da Silva-Diz V, Munoz P, et al. (2011). The intestinal stem cell signature identifies colorectal cancer stem cells and predicts disease relapse. Cell Stem Cell 8, 511–524. [PubMed: 21419747]

Montoro DT, Haber AL, Biton M, Vinarsky V, Lin B, Birket SE, Yuan F, Chen S, Leung HM, Villoria J, et al. (2018). A revised airway epithelial hierarchy includes CFTR-expressing ionocytes. Nature 560, 319–324. [PubMed: 30069044]

Nabhan AN, Brownfield DG, Harbury PB, Krasnow MA, and Desai TJ (2018). Single-cell Wnt signaling niches maintain stemness of alveolar type 2 cells. Science 359, 1118–1123. [PubMed: 29420258]

Nagendran M, Riordan DP, Harbury PB, and Desai TJ (2018). Automated cell-type classification in intact tissues by single-cell molecular profiling. Elife 7.

Nettesheim P, and Martin DH (1970). Appearance of glandlike structures in the tracheobronchial tree of aging mice. J Natl Cancer Inst 44, 687–693. [PubMed: 11515437]

Oliveira MJ, Pereira AS, Guimaraes L, Grande NR, de Sa CM, and Aguas AP (2003). Zonation of ciliated cells on the epithelium of the rat trachea. Lung 181, 275–282. [PubMed: 14705771]

Ooi AT, Mah V, Nickerson DW, Gilbert JL, Ha VL, Hegab AE, Horvath S, Alavi M, Maresh EL, Chia D, et al. (2010). Presence of a putative tumor-initiating progenitor cell population predicts poor prognosis in smokers with non-small cell lung cancer. Cancer Res 70, 6639–6648. [PubMed: 20710044]

Paul MK, Bisht B, Darmawan DO, Chiou R, Ha VL, Wallace WD, Chon AT, Hegab AE, Grogan T, Elashoff DA, et al. (2014). Dynamic changes in intracellular ROS levels regulate airway basal stem cell homeostasis through Nrf2-dependent Notch signaling. Cell Stem Cell 15, 199–214. [PubMed: 24953182]

Plasschaert LW, Zilionis R, Choo-Wing R, Savova V, Knehr J, Roma G, Klein AM, and Jaffe AB (2018). A single-cell atlas of the airway epithelium reveals the CFTR-rich pulmonary ionocyte. Nature 560, 377–381. [PubMed: 30069046]

Rawlins EL, Okubo T, Xue Y, Brass DM, Auten RL, Hasegawa H, Wang F, and Hogan BL (2009). The role of Scgb1a1+ Clara cells in the long-term maintenance and repair of lung airway, but not alveolar, epithelium. Cell Stem Cell 4, 525–534. [PubMed: 19497281]

Reynolds SD, Zemke AC, Giangreco A, Brockway BL, Teisanu RM, Drake JA, Mariani T, Di PY, Taketo MM, and Stripp BR (2008). Conditional stabilization of beta-catenin expands the pool of lung stem cells. Stem Cells 26, 1337–1346. [PubMed: 18356571]

Rhee J, Buchan T, Zukerberg L, Lilien J, and Balsamo J (2007). Cables links Robo-bound Abl kinase to N-cadherin-bound beta-catenin to mediate Slit-induced modulation of adhesion and transcription. Nat Cell Biol 9, 883–892. [PubMed: 17618275]

Rock JR, Gao X, Xue Y, Randell SH, Kong YY, and Hogan BL (2011). Notch-dependent differentiation of adult airway basal stem cells. Cell Stem Cell 8, 639–648. [PubMed: 21624809]

Rock JR, Onaitis MW, Rawlins EL, Lu Y, Clark CP, Xue Y, Randell SH, and Hogan BL (2009). Basal cells as stem cells of the mouse trachea and human airway epithelium. Proc Natl Acad Sci U S A 106, 12771–12775. [PubMed: 19625615]

Rock JR, Randell SH, and Hogan BL (2010). Airway basal stem cells: a perspective on their roles in epithelial homeostasis and remodeling. Dis Model Mech 3, 545–556. [PubMed: 20699479]

Rubinfeld B, Albert I, Porfiri E, Fiol C, Munemitsu S, and Polakis P (1996). Binding of GSK3beta to the APC-beta-catenin complex and regulation of complex assembly. Science 272, 1023–1026. [PubMed: 8638126]

Schoch KG, Lori A, Burns KA, Eldred T, Olsen JC, and Randell SH (2004). A subset of mouse tracheal epithelial basal cells generates large colonies in vitro. Am J Physiol Lung Cell Mol Physiol 286, L631–642. [PubMed: 12959927]

Tadokoro T, Gao X, Hong CC, Hotten D, and Hogan BL (2016). BMP signaling and cellular dynamics during regeneration of airway epithelium from basal progenitors. Development 143, 764–773. [PubMed: 26811382]

Tadokoro T, Wang Y, Barak LS, Bai Y, Randell SH, and Hogan BL (2014). IL-6/STAT3 promotes regeneration of airway ciliated cells from basal stem cells. Proc Natl Acad Sci U S A 111, E3641–3649. [PubMed: 25136113]

Tammela T, Sanchez-Rivera FJ, Cetinbas NM, Wu K, Joshi NS, Helenius K, Park Y, Azimi R, Kerper NR, Wesselhoeft RA, et al. (2017). A Wnt-producing niche drives proliferative potential and progression in lung adenocarcinoma. Nature 545, 355–359. [PubMed: 28489818]

Tata A, Kobayashi Y, Chow RD, Tran J, Desai A, Massri AJ, McCord TJ, Gunn MD, and Tata PR (2018). Myoepithelial Cells of Submucosal Glands Can Function as Reserve Stem Cells to Regenerate Airways after Injury. Cell Stem Cell 22, 668–683 e666. [PubMed: 29656943]

Tata PR, Mou H, Pardo-Saganta A, Zhao R, Prabhu M, Law BM, Vinarsky V, Cho JL, Breton S, Sahay A, et al. (2013). Dedifferentiation of committed epithelial cells into stem cells in vivo. Nature 503, 218–223. [PubMed: 24196716]

Toskala E, Smiley-Jewell SM, Wong VJ, King D, and Plopper CG (2005). Temporal and spatial distribution of ciliogenesis in the tracheobronchial airways of mice. Am J Physiol Lung Cell Mol Physiol 289, L454–459. [PubMed: 15879461]

Volckaert T, Dill E, Campbell A, Tiozzo C, Majka S, Bellusci S, and De Langhe SP (2011). Parabronchial smooth muscle constitutes an airway epithelial stem cell niche in the mouse lung after injury. J Clin Invest 121, 4409–4419. [PubMed: 21985786]

Walentek P, Beyer T, Hagenlocher C, Muller C, Feistel K, Schweickert A, Harland RM, and Blum M (2015). ATP4a is required for development and function of the Xenopus mucociliary epidermis - a potential model to study proton pump inhibitor-associated pneumonia. Dev Biol 408, 292–304. [PubMed: 25848696]

Walentek P, Beyer T, Thumberger T, Schweickert A, and Blum M (2012). ATP4a is required for Wnt-dependent Foxj1 expression and leftward flow in Xenopus left-right development. Cell Rep 1, 516–527. [PubMed: 22832275]

Wang F, Flanagan J, Su N, Wang LC, Bui S, Nielson A, Wu X, Vo HT, Ma XJ, and Luo Y (2012). RNAscope: a novel in situ RNA analysis platform for formalin-fixed, paraffin-embedded tissues. The Journal of molecular diagnostics : JMD 14, 22–29. [PubMed: 22166544]

Wansleeben C, Bowie E, Hotten DF, Yu YR, and Hogan BL (2014). Age-related changes in the cellular composition and epithelial organization of the mouse trachea. PLoS One 9, e93496. [PubMed: 24675804]

Wine JJ, and Joo NS (2004). Submucosal glands and airway defense. Proceedings of the American Thoracic Society 1, 47–53. [PubMed: 16113412]

Yost C, Torres M, Miller JR, Huang E, Kimelman D, and Moon RT (1996). The axis-inducing activity, stability, and subcellular distribution of beta-catenin is regulated in Xenopus embryos by glycogen synthase kinase 3. Genes Dev 10, 1443–1454. [PubMed: 8666229]

Zepp JA, Zacharias WJ, Frank DB, Cavanaugh CA, Zhou S, Morley MP, and Morrisey EE (2017). Distinct Mesenchymal Lineages and Niches Promote Epithelial Self-Renewal and Myofibrogenesis in the Lung. Cell 170, 1134–1148 e1110. [PubMed: 28886382]

Highlights

- Tracheal epithelial β-catenin tightly controls proliferation and differentiation
- PDGFRα+ lineage comprises Wnt signaling niche necessary for epithelial proliferation
- Airway basal stem cell-derived Wnts facilitate differentiation to ciliated cells
- Age-related Wnt/β-catenin niche changes drive gland-like epithelial invaginations

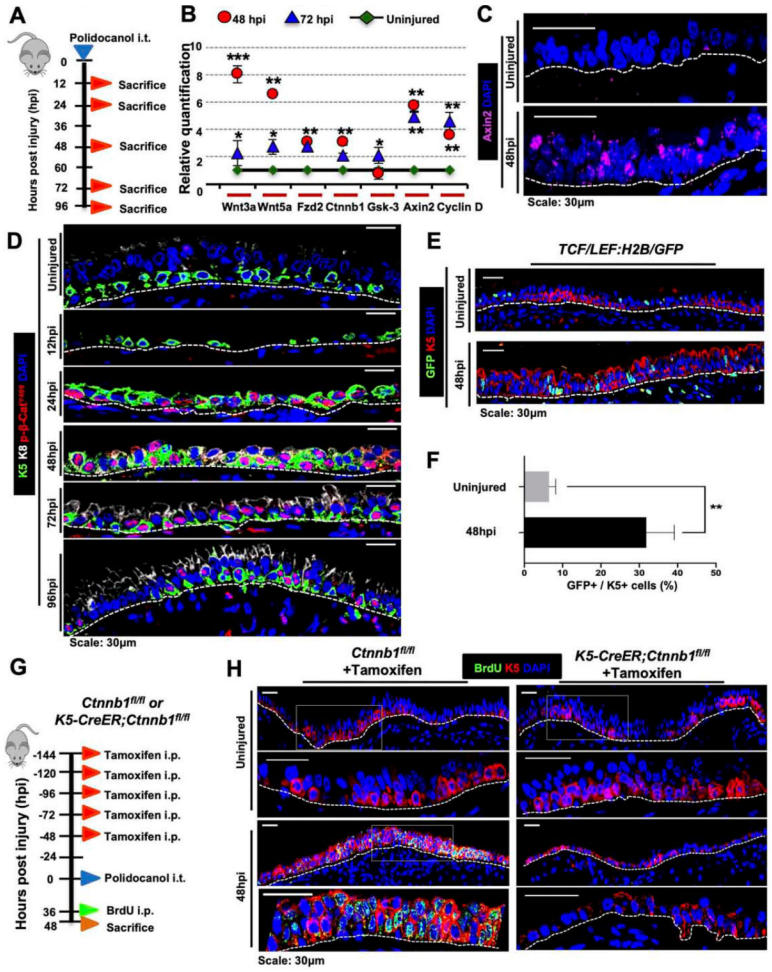

Figure 1. Canonical Wnt/β-catenin signaling is essential for proximal ABSC proliferation after injury *in vivo*.

A. Experimental schematic outlining intratracheal (i.t.) administration of polidocanol to wild type 6–10-week-old mice and euthanasia timeline post-injury.

B. qRT-PCR assessing mRNA expression levels of several components and targets of the Wnt/β-catenin signaling pathway from stripped tracheal epithelia of mice at varying timepoints post-polidocanol injury.

C. Images of *in situ* hybridization in uninjured and 48hpi wildtype mouse tracheas using probes targeting *Axin2* mRNA.

D. IF images of p-β-catenin^{Y489} (red) in uninjured and repairing mouse tracheal epithelia at varying timepoints post-injury.

E. IF images of *TCF/Lef:H2B/GFP* reporter mice with and without polidocanol injury.

F. Quantification of percentage of K5+ GFP+ cells in the surface airway epithelium of *TCF/Lef:H2B/GFP* reporter mice with and without polidocanol injury.

G. Experimental schematic outlining tamoxifen administration, i.t. polidocanol injury, BrdU administration, and euthanasia of *Ctnnb1$^{fl/fl}$* and *K5-CreER;Ctnnb1$^{fl/fl}$* transgenic mice.

H. IF images of uninjured and 48hpi mouse airway epithelia of *Ctnnb1$^{fl/fl}$* and *K5-CreER;Ctnnb1$^{fl/fl}$* transgenic mice assessing BrdU incorporation. Bottom images of a given timepoint are magnifications of outlined white box in top images.

Bar graph represents SEM, n = 3–6. *p < 0.05, *** p < 0.001 by Student's t test.

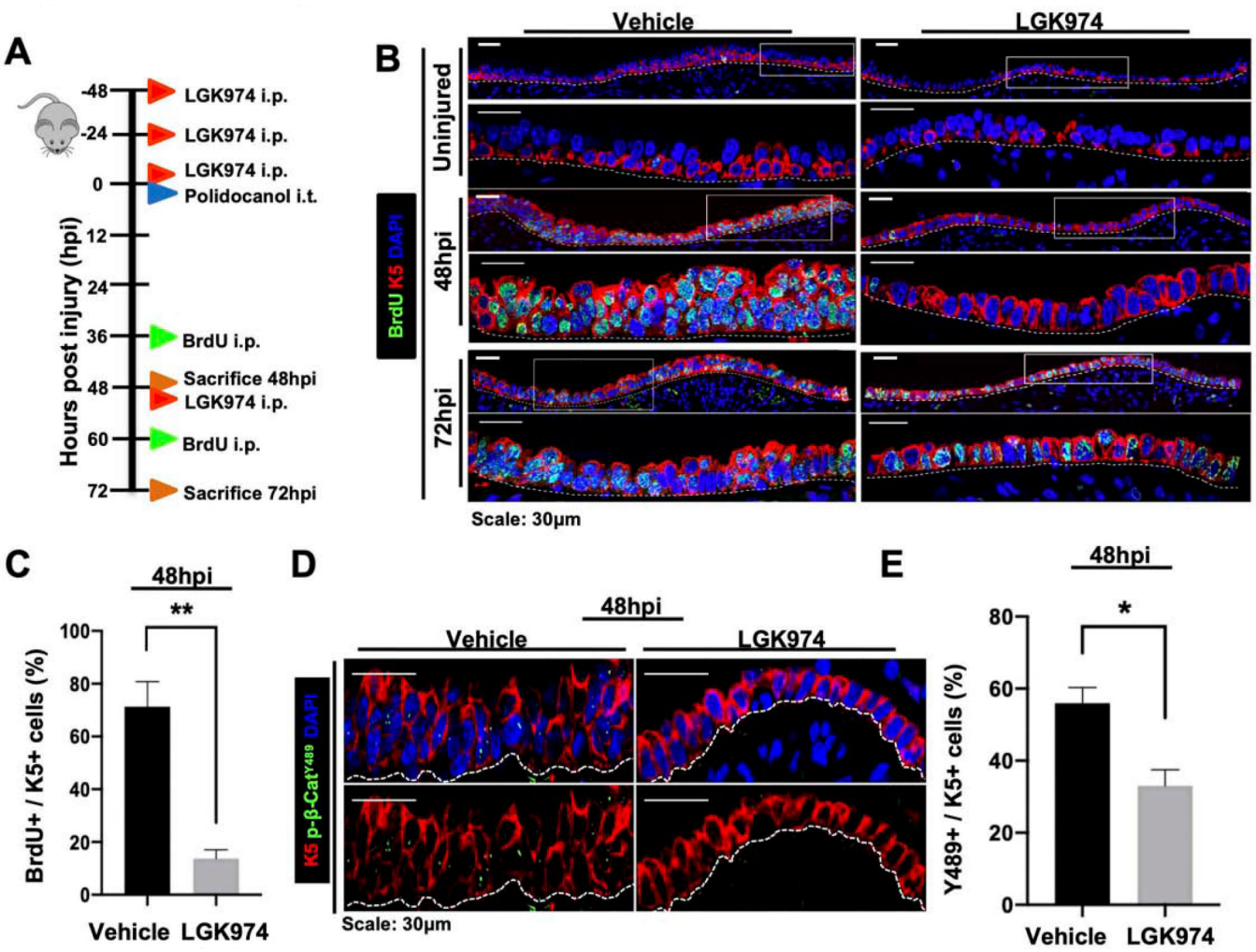

Figure 2. Porcupine-dependent phosphorylation of β-catenin at Y489 regulates ABSC proliferation.

A. Experimental schematic outlining vehicle or LGK974 treatment, i.t. polidocanol injury, BrdU administration, and euthanasia of 6–10-week-old mice.

B. IF images of uninjured, 48hpi, and 72hpi mouse airway epithelia wild type mice treated with vehicle or LGK974 assessing BrdU incorporation. Bottom images of a given timepoint are magnifications of outlined white box in top images.

C. Quantifications of percentage of proliferating BrdU+ K5+ mABSCs at 48hpi from mice treated with vehicle or LGK974.

D. IF images of 48hpi mouse airway epithelia wild type mice treated with vehicle or LGK974 assessing nuclear p-β-catenin^{Y489} in the SAE.

E. Quantifications of percentage of K5+ mABSCs with nuclear p-β-catenin^{Y489} in tracheas of mice at 48hpi treated with vehicle or LGK974.

Bar graph represents SEM, n = 3–6. *p < 0.05, ** p < 0.01, *** p < 0.001 by Student's t test.

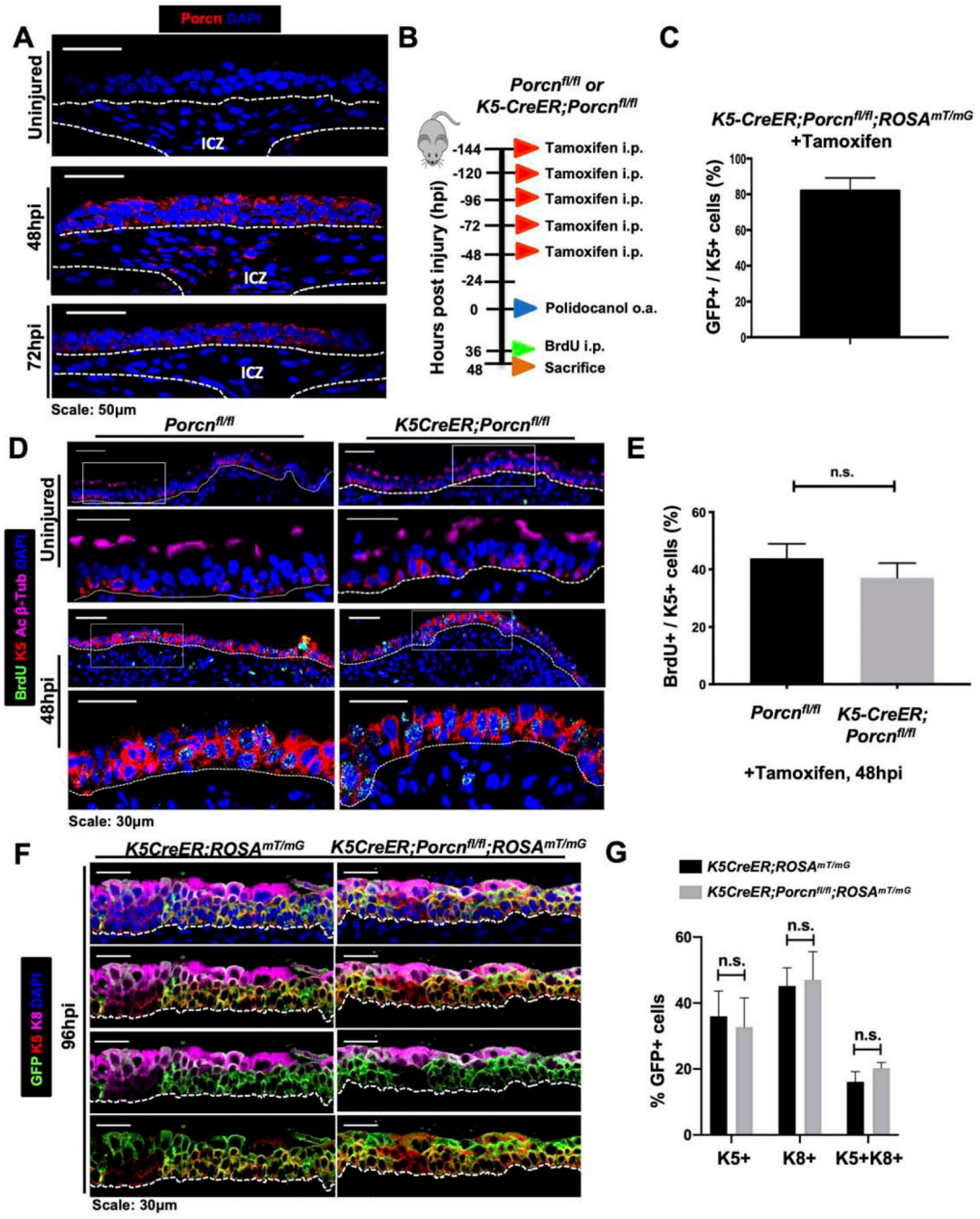

Figure 3. ABSC-derived Wnt secretion is dispensable for ABSC proliferation and early progenitor cell formation following injury *in vivo.*

A. IF images of Porcupine (red) in wild type uninjured and repairing airway epithelia. ICZ = Intercartilaginous zone.

B. Experimental schematic outlining tamoxifen administration, oropharyngeal aspiration (o.a.) of polidocanol injury, BrdU administration, and euthanasia of *Porcn*$^{fl/fl}$ and *K5-CreER;Porcn*$^{fl/fl}$ transgenic mice.

C. Quantification of percentage of K5+ GFP+ double-positive cells that are from *K5-CreER;Porcn*$^{fl/fl}$ transgenic mice treated with tamoxifen as outlined in Figure 3B.

D. IF images of uninjured and 48hpi mouse airway epithelia of *Porcn*$^{fl/fl}$ and *K5-CreER;Porcn*$^{fl/fl}$ transgenic mice assessing BrdU incorporation. Bottom images of a given timepoint are magnifications of outlined white box in top images.

E. Quantification of percentage of BrdU+ K5+ mABSCs at 48hpi of *Porcn*$^{fl/fl}$ and *K5-CreER;Porcn*$^{fl/fl}$ transgenic mice. n.s. = not significant.

F. IF images of uninjured, 48hpi, 72hpi, and 96hpi mouse airway epithelia of *Porcn*$^{fl/fl}$ and *K5-CreER;Porcn*^{fm} transgenic mice assessing emergence K8+ early progenitors.

G. Quantification of percentage of K8+ early progenitors from uninjured, 48hpi, 72hpi, and 96hpi mouse airway epithelia of *Porcn*$^{fl/fl}$ and *K5-CreER;Porcn*$^{fl/f}$ transgenic mice.

Bar graph represents SEM, n = 3–6. *p < 0.05, ** p < 0.01, *** p < 0.001 by Student's t test.

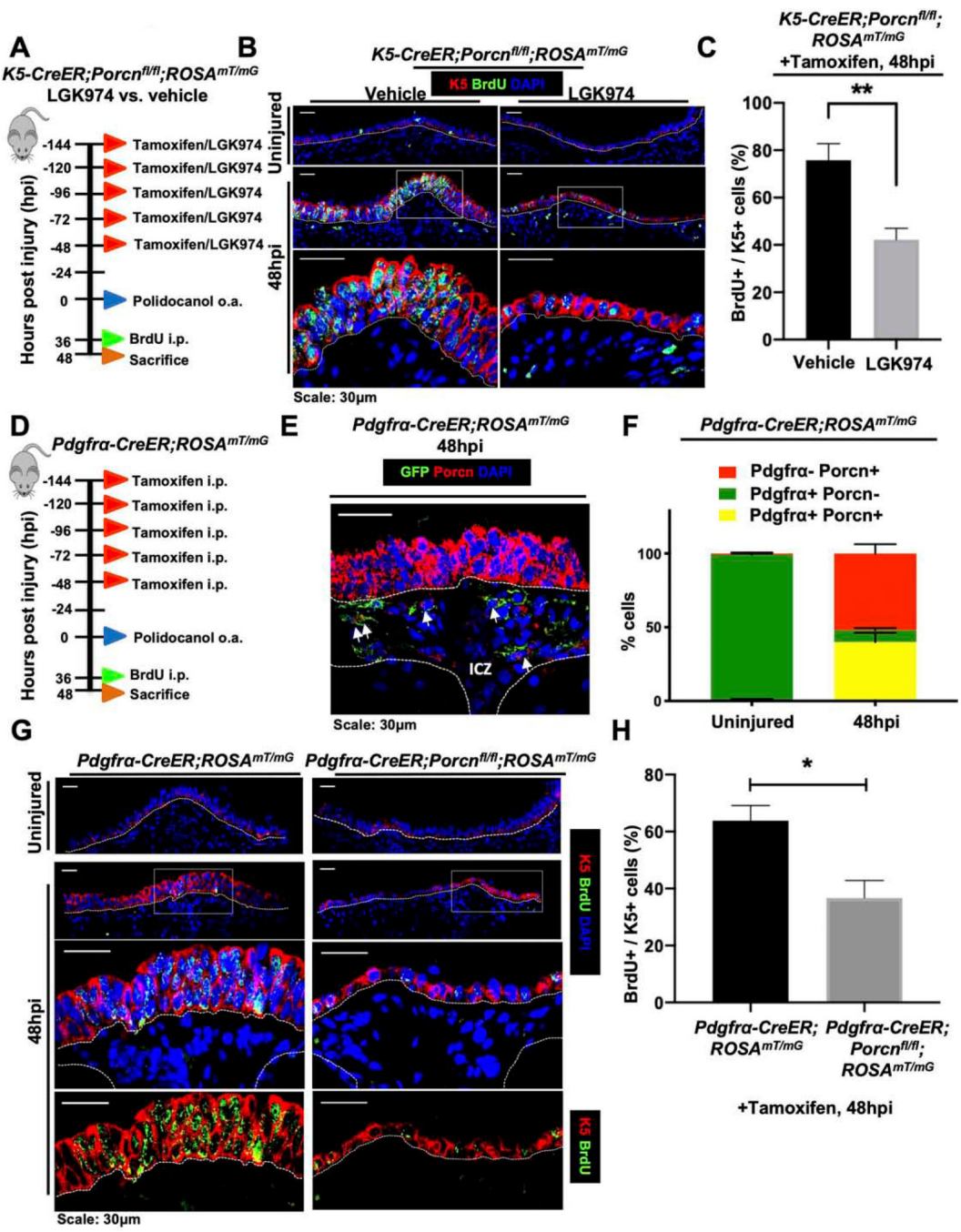

Figure 4. The ICZ Pdgfrα+ lineage is a critical source of Wnt ligand for ABSC proliferation *in vivo*.

A. Experimental schematic outlining tamoxifen administration, oropharyngeal aspiration (o.a.) of polidocanol injury, BrdU administration, and euthanasia of *K5-CreER;Porcn$^{fl/fl}$;ROSA$^{mT/mG}$* transgenic mice treated with vehicle or LGK974 prior to injury.

B. IF images of uninjured and 48hpi mouse airway epithelia of *K5-CreER;Porcn$^{fl/fl}$;ROSA$^{mT/mG}$* transgenic mice treated with vehicle or LGK974 assessing

BrdU incorporation. Bottom images of a given timepoint are magnifications of outlined white box in top images.

C. Quantification of percentage of BrdU+ K5+ at 48hpi of *K5-CreER;Porcn$^{fl/fl}$;ROSA$^{mT/mG}$* transgenic mice treated with vehicle or LGK974.

D. Experimental schematic outlining tamoxifen administration, oropharyngeal aspiration (o.a.) of polidocanol injury, BrdU administration, and euthanasia of *Pdgfra-CreER;ROSA$^{mT/mG}$* transgenic mice.

E. IF image of GFP (green; Pdgfrα+ lineage) in *Pdgfra-CreER;ROSA$^{mT/mG}$* mice at 48hpi co-stained with Porcupine (red).

F. Quantification of percentage of Pdgfrα+ Porcn+, Pdgfrα+ Porcn-, and Pdgfrα- Porcn+ cells in the ICZ of Pdgfrα-CreER;ROSA$^{mT/mG}$ mice that were uninjured or 48hpi.

G. IF images of uninjured and 48hpi mouse airway epithelia of *Pdgfra-CreER;ROSA$^{mT/mG}$* and *Pdgfra-CreER;Porcn$^{fl/fl}$;ROSA$^{mT/mG}$* transgenic mice assessing BrdU incorporation. Bottom images of a given timepoint are magnifications of outlined white box in top images.

H. Quantification of percentage of BrdU+ K5+ at 48hpi of *Pdgfra-CreER;ROSA$^{mT/mG}$* and *Pdgfra-CreER;Porcn$^{fl/fl}$;ROSA$^{mT/mG}$* transgenic mice.

Bar graph represents SEM, n = 3–6. *p < 0.05, ** p < 0.01, *** p < 0.001 by Student's t test.

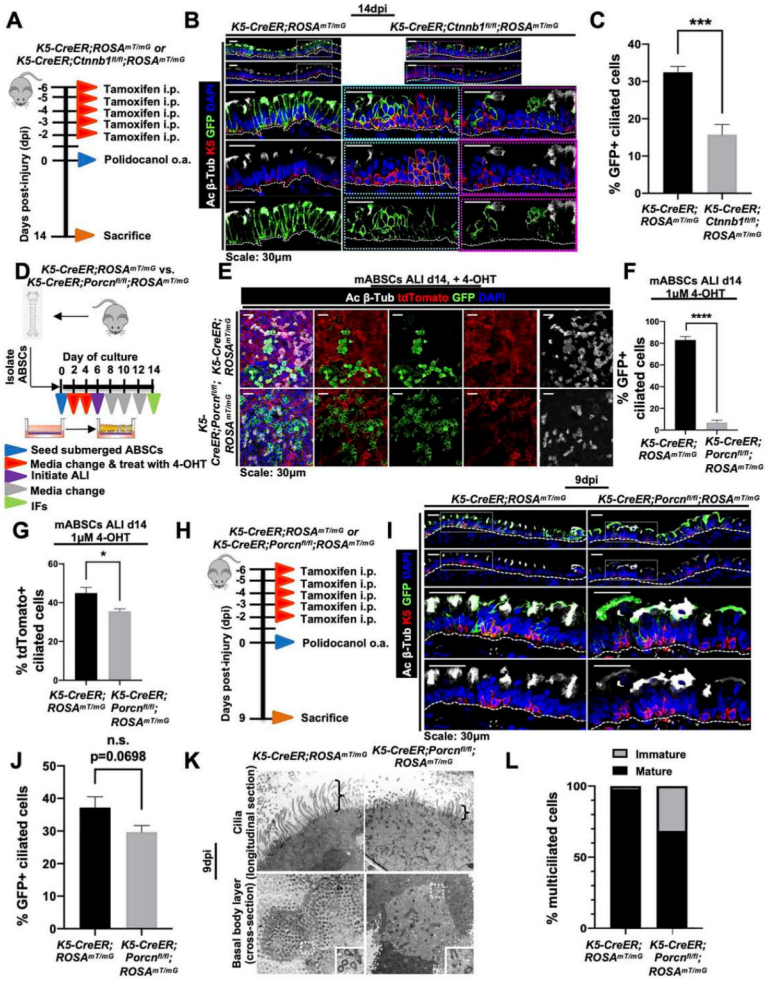

Figure 5. ABSC-derived Wnt secretion is necessary for differentiation to the ciliated cell fate.

A. Experimental schematic outlining tamoxifen administration, oropharyngeal aspiration (o.a.) of polidocanol injury, and euthanasia of *K5-CreER;ROSA*$^{mT/mG}$ and *K5-CreER;Ctnnb1*$^{fl/fl}$*;ROSA*$^{mT/mG}$ transgenic mice at 14 days post-injury (dpi).

B. IF images of *K5-CreER;ROSA*$^{mT/mG}$ and *K5-CreER;Ctnnb1*$^{fl/fl}$*;ROSA*$^{mT/mG}$ transgenic mice at 14dpi assessing GFP+ lineage differentiation the ciliated cell fate. Bottom images are magnifications of outlined white box in top images for *K5-CreER;ROSA*$^{mT/mG}$ mice. For *K5-CreER;Ctnnb1*$^{fl/fl}$*;ROSA*$^{mT/mG}$ transgenic, bottom images are magnifications of indicated cyan or magenta outlined boxes from top images.

C. Quantification of percentage of GFP+ lineage-traced ciliated cells from *K5-CreER;ROSA*$^{mT/mG}$ and *K5-CreER;Ctnnb1*$^{fl/fl}$*;ROSA*$^{mT/mG}$ transgenic mice at 14dpi.

D. Experimental schematic outlining isolation and culture of *K5-CreER;ROSA*$^{mT/mG}$ and *K5-CreER;Porcn*$^{fl/fl}$*;ROSA*$^{mT/mG}$ mABSCs, treatment with 4-OHT and initiation of ALI.

E. IF images of mASBCs treated with 4-OHT from *K5-CreER;ROSA*$^{mT/mG}$ and *K5-CreER;Porcn*$^{fl/fl}$*;ROSA*$^{mT/mG}$ mice tracheas on ALI day 14 assessing GFP+ lineage differentiation to the ciliated cell fate.

F. Quantification of percentage of GFP+ lineage-traced ciliated cells from *K5-CreER;ROSA*$^{mT/mG}$ and *K5-CreER;Porcn*$^{fl/fl}$*;ROSA*$^{mT/mG}$ mABSCs on ALI day 14.

G. Quantification of percentage of GFP- lineage-traced ciliated cells from *K5-CreER;ROSA$^{mT/mG}$* and *K5-CreER;Porcn$^{fl/fl}$;ROSA$^{mT/mG}$* mABSCs on ALI day 14.
H. Experimental schematic outlining tamoxifen administration, oropharyngeal aspiration (o.a.) of polidocanol injury, and euthanasia of *K5-CreER;ROSA$^{mT/mG}$* and *K5-CreER;Porcn$^{fl/fl}$;ROSA$^{mT/mG}$* transgenic mice at 9dpi.
I. IF images of *K5-CreER;ROSA$^{mT/mG}$* and *K5-CreER;Porcn$^{fl/fl}$;ROSA$^{mT/mG}$* transgenic mice at 9dpi assessing GFP+ lineage differentiation to ciliated cell fate. Bottom images of a given timepoint are magnifications of outlined white box in top images.
J. Quantification of percentage of GFP+ lineage-traced ciliated cells from *K5-CreER;ROSA$^{mT/mG}$* and *K5*-CreER;Porcn$^{fl/fl}$;ROSA$^{mT/mG}$ *transgenic mice at 9dpi.*
K. TEM images of *K5-CreER;ROSA$^{mT/mG}$* and *K5-CreER;Porcn$^{fl/fl}$;ROSA$^{mT/mG}$* transgenic mice tracheal longitudinal thin sections at 9dpi. Brackets show axonemal height of wildtype and mutant cells.
L. Quantification of percentage of mature and immature ciliated cells by TEM in *K5-CreER;ROSA$^{mT/mG}$* and *K5-CreER;Porcn$^{fl/fl}$;ROSA$^{mT/mG}$* transgenic mice tracheas at 9dpi. Bar graph represents SEM, n = 3–6. *p < 0.05, ** p < 0.01, *** p < 0.001 by Student's t test.

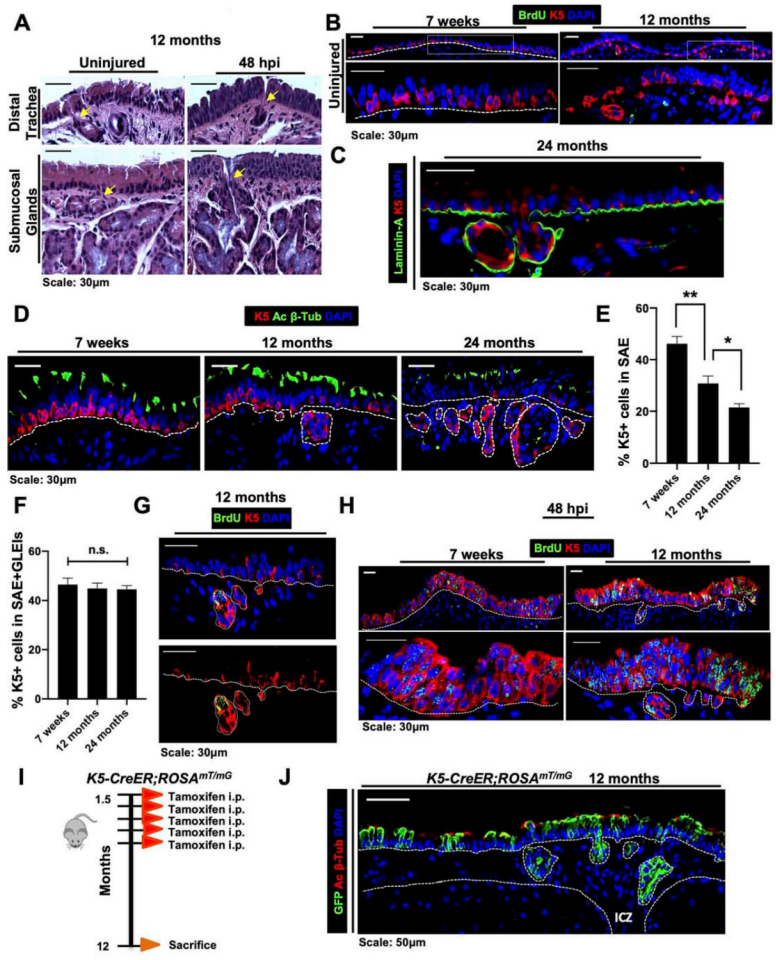

Figure 6. Glandular-like epithelial invaginations emerge exclusively in the ICZ during aging, arise from ABSCs, and contribute to homeostasis and repair.

A. H&E images of uninjured and 48hpi 12-month-old mouse tracheas showing glandular-like epithelial invaginations (GLEIs) and submucosal glands with ducts connecting to surface airway epithelium (yellow arrows).

B. IF images of uninjured 12-month-old mouse tracheas that including K5+ staining in GLEIs. Bottom images of a given timepoint are magnifications of outlined white box in top images.

C. IF image of GLEIs in 24-month old mice for basement membrane marker Laminin-A (green).

D. IF images of the airway from mice at varying ages for K5 and acetylated β-tubulin.

E. Quantifications of percentage of K5+ cells in the SAE during aging.

F. Quantifications of percentage of K5+ cells in the SAE and GLEIs during aging.

G. IF images of GLEIs from 12-month old uninjured mice that were administered a 12-hour BrdU pulse prior to euthanasia.

H. IF images of tracheal epithelia at 48hpi in 7-week-old versus 12-month-old mice assessing localization of proliferation by BrdU incorporation.

I. Experimental schematic outlining tamoxifen administration of *K5-CreER;ROSA*$^{mT/mG}$ transgenic mice to label K5+ ABSCs during youth and timeline of euthanasia during aging.

J. IF image of *K5-CreER;ROSA*$^{mT/mG}$ transgenic mouse tracheal epithelia showing GLEIs at 12 months after administration of tamoxifen at 1.5 months of age.
Bar graph represents SEM, *p < 0.05, ** p < 0.01, *** p < 0.001, n.s. = not significant by Student's t test.

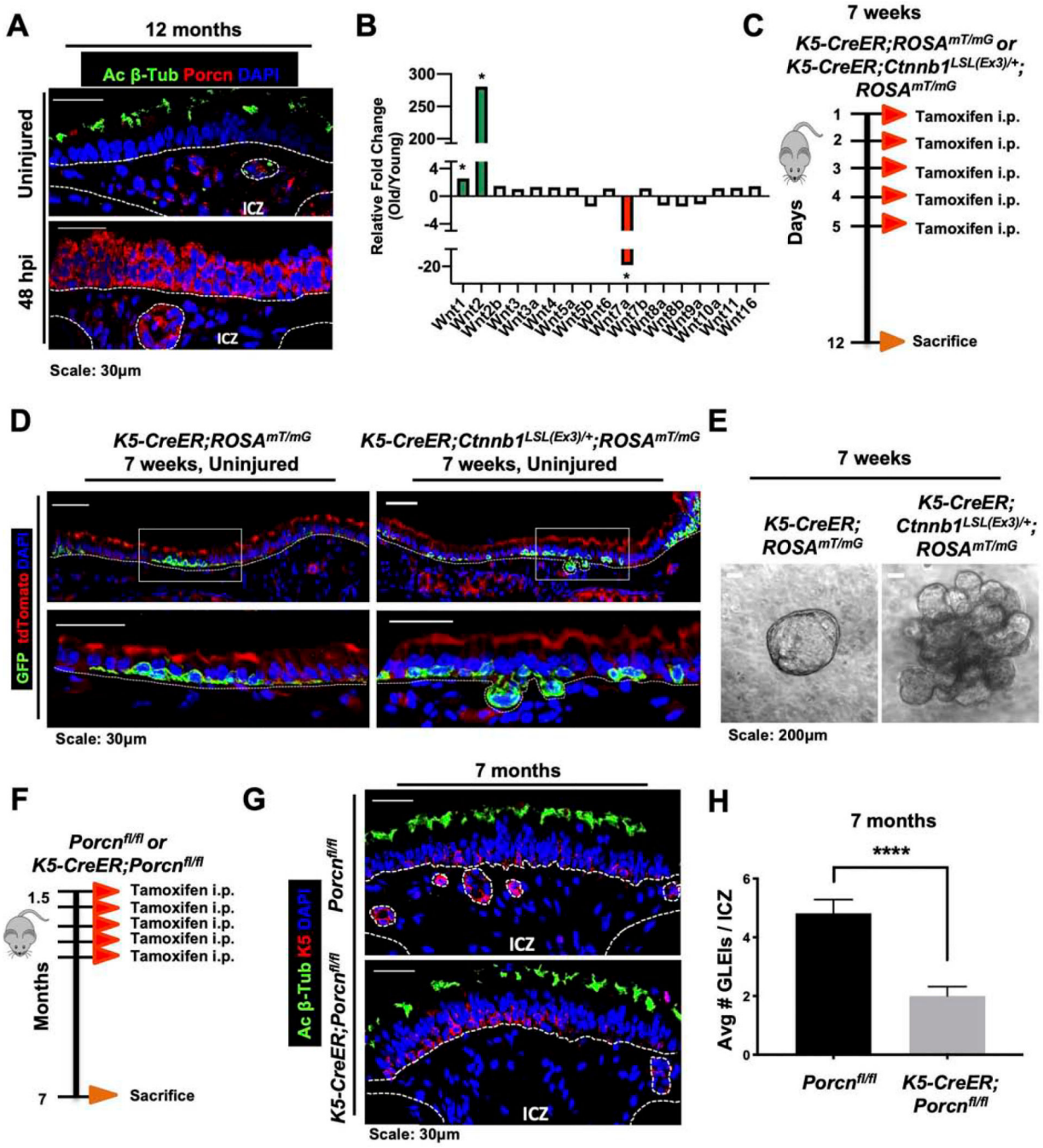

Figure 7. A dynamic ABSC Wnt-secreting niche facilitates GLEI formation during aging *in vivo*.

A. IF images of Porcupine (red) in uninjured and 48hpi 12-month-old mouse tracheas.

B. qRT-PCR data showing fold changes of Wnt ligand expression in RNA isolated from stripped airway epithelia of 12-month-old mice versus 7-week-old mice.

C. Experimental schematic outlining tamoxifen administration and euthanasia of *K5-CreER;ROSA*$^{mT/mG}$ or *K5-CreER;Ctnnb1*$^{LSL(Ex)/+}$*;ROSA*$^{mT/mG}$ mice at 7 weeks of ages.

D. IF images of tdTomato (red) and GFP (green; K5+ lineage) of uninjured *K5-CreER;ROSA*$^{mT/mG}$ or *K5-CreER;Ctnnb1*$^{LSL(Ex)/+}$*;ROSA*$^{mT/mG}$ transgenic mouse airway

epithelia. Bottom images of a given timepoint are magnifications of outlined white box in top images.

E. Brightfield images of tracheospheres grown *in vitro* from *K5-CreER;ROSA*$^{mT/mG}$ or *K5-CreER;Ctnnb1*$^{LSL(Ex)/+}$*;ROSA*$^{mT/mG}$ mice at 7 weeks of age following tamoxifen administration *in vivo.*

F. Experimental schematic outlining tamoxifen administration of *Porcn*$^{fl/fl}$ or *K5-CreER;Porcn*$^{fl/fl}$ transgenic mice to induce recombination K5+ ABSCs during youth and timeline of euthanasia during aging.

G. IF images of *Porcn*$^{fl/fl}$ or *K5-CreER;Porcn*$^{fl/fl}$ transgenic mouse airway epithelia at 7 months when administered tamoxifen at 1.5 months of age showing GLEIs.

H. Quantification of average number of GLEIs per ICZ region from *Porcn*$^{fl/fl}$ or *K5-CreER;Porcn*^{fm} transgenic mice at 7 months when administered tamoxifen at 1.5 months of age.

Bar graph represents SEM, n = 3–6. *p < 0.05, ** p < 0.01, *** p < 0.001 by Student's t test.

Key Resources Table

REAGENT or RESOURCE	SOURCE	IDENTIFIER
Antibodies		
Goat anti-mouse TROP2-APC	R&D	Cat# AF1122; RRID:AB_2205662
Rat anti-mouse ITGA6-PE	BioLegend	Cat# 313611; RRID:AB_893374
Rabbit Keratin 5	Covance	Cat # PRB-160P; RRID:AB_291581
Chicken Keratin 5	Covance	Cat# SIG-3475; RRID:AB_10720202
Rat Keratin 8	DSHB	Cat# TROMA-I; RRID:AB_531826
Mouse GSK3β	Abcam	Cat# ab93926; RRID:AB_10563643
Mouse Acetylated β-Tubulin	Sigma	Cat# T7451; RRID:AB_609894
Rat BrdU	Abcam	Cat# ab6326; RRID:AB_305426
Rabbit Porcupine	Abcam	Cat# ab105543; RRID:AB_10860951
Mouse Porcupine	Millipore-Sigma	Cat# MABS21; RRID:AB_11203317
Rabbit Laminin-A	ThermoFisher	Cat# PA5–16287; RRID:AB_10985513
Rabbit Total β-catenin	Abcam	Cat# ab32572; RRID:AB_725966
Mouse p-β-catenin^{Y489}	DSHB	Cat# PY489-B-catenin; RRID:AB_10144551
Rabbit p-β-catenin^{S33,S37,T41}	Cell Signaling Technology	Cat# 9561T; RRID:AB_331729
Rabbit p-β-catenin^{S675}	Cell Signaling Technology	Cat# 4176; RRID:AB_1903923
Chicken GFP	Abcam	Cat# ab13970; RRID:AB_300798
Rat tdTomato	Kerafast	Cat# EST203; RRID:AB_2732803
Goat anti-Rabbit IgG (H+L) Highly Cross-Adsorbed Secondary Antibody, Alexa Fluor 594	ThermoFisher	Cat# A-11037; RRID:AB_2534095
Goat anti-Mouse IgG (H+L) Highly Cross-Adsorbed Secondary Antibody, Alexa Fluor 488	ThermoFisher	Cat# A-11029; RRID:AB_138404
Goat anti-Chicken IgY (H+L) Secondary Antibody, Alex Fluor 488	ThermoFisher	Cat# A-11039; RRID:AB_142924
Goat anti-Rat IgG (H+L) Cross-Adsorbed Secondary Antibody, Alexa Fluor 647	ThermoFisher	Cat# A-21247; RRID:AB_141778
Biological Samples		
Human bronchiolar airway tissue specimens	Ronald Reagan UCLA Medical Center	N/A
Chemicals, Peptides, and Recombinant Proteins		
Tamoxifen	Sigma	Cat# T5648
BrdU	Sigma	Cat# B5002
(Z)-4-Hydroxytamoxifen (4-OHT)	Sigma	Cat# H7904
LGK974	MedChem Express	Cat# HY-17545
Dispase	Corning	Cat# 354235
Collagen type I	Corning	Cat# 354249
HEPES	Sigma	Cat# H0887
Sodium Bicarbonate	Life Technologies	Cat# 25080–094
L-glutamine	Invitrogen	Cat# 35050–061
Insulin	Sigma	Cat# I6634

REAGENT or RESOURCE	SOURCE	IDENTIFIER
Transferrin	Sigma	Cat# T5391
Cholera Toxin	Sigma	Cat# C8052
Epidermal Growth Factor (EGF)	Corning	Cat# 354001
Bovine Pituitary Extract	Invitrogen	Cat# 13028–014
Fetal Bovine Serum	ThermoFisher	Cat# SH3008803HI
Bovine Serum Albumin	ThermoFisher	Cat# BP9706
Retinoic Acid	Sigma	Cat# R2625
Polidocanol	Sigma	Cat# P9641
Critical Commercial Assays		
Click-iT EdU Incorporation Assay Kit	Invitrogen	Cat# C10337
Mouse Wnt Signaling Pathway RT^2 Profiler PCR Array	Qiagen	Cat# PAMM-043Z
Experimental Models: Organisms/Strains		
Mouse: C57BL/6J	The Jackson Laboratory	JAX Stock# 000664
Mouse: *K5-CreER^{T2}*	The Jackson Laboratory	JAX Stock# 029155
Mouse: *ROSA$^{mT/mG}$*	The Jackson Laboratory	JAX Stock# 007576
Mouse: *Porcn$^{fl/fl}$*	The Jackson Laboratory	JAX Stock# 020944
Mouse: *Pdgfrα-CreER^{TM}*	The Jackson Laboratory	JAX Stock# 018280
Mouse: *Ctnnb1$^{fl/fl}$*	The Jackson Laboratory	JAX Stock# 004152
Mouse: *K8-CreER^{T2}*	The Jackson Laboratory	JAX Stock# 017947
Mouse: *TCF/Lef:H2B/GFP*	The Jackson Laboratory	JAX Stock# 013752
Mouse: *Ctnnb1$^{LSL(Ex3)/+}$*	Van Andel Institute, U.S.	Kind gift from Mark Taketo via Bart Williams
Oligonucleotides		
Primers for genotyping of mouse lines, see Table S1	This paper	N/A
qPCR TaqMan probes, see Table S5	This paper	N/A
Software and Algorithms		
GraphPad Prism 7	GraphPad Software	RRID:SCR_002798
Fiji	ImageJ	RRID:SCR_002285
Other		
PLISH probe: *Axin2*	Nabhan et al. 2018	N/A